https://doi.org/10.5194/tc-2021-249
Preprint. Discussion started: 16 August 2021

The Cryosphere Discussions

A new sea ice state dependent parameterization for the free drift of sea ice

Charles Brunette[1], L. Bruno Tremblay[1], and Robert Newton[2]

[1]Department of Atmospheric & Oceanic Sciences, McGill University, Montreal, QC, Canada
[2]Lamont-Doherty Earth Observatory, Columbia University, Palisades, NY, USA

Correspondence: Charles Brunette (charles.brunette@mail.mcgill.ca)

Abstract. Free drift estimates of sea ice motion are necessary to produce a seamless observational record combining buoy and satellite-derived sea ice motion vectors. We develop a new parameterization for the free drift of sea ice based on wind forcing, wind turning angle, sea ice state variables (concentration and thickness) and ocean current (as a residual). Building on the fact that the spatially varying standard wind-ice transfer coefficient (considering only surface wind stress) has a structure as the spatial distribution of sea ice thickness, we introduce a wind-ice transfer coefficient that scales linearly with thickness. Results show a mean error of -0.5 cm/s (low-speed bias) and a root-mean-square error of 5.1 cm/s, considering daily buoy drift data as truth. This represents a 31% reduction of the error on drift speed compared to the free drift estimates used in the Polar Pathfinder dataset (Tschudi et al., 2019). The thickness-dependent wind transfer coefficient provides an improved seasonality and long-term trend of the sea ice drift speed, with a minimum (maximum) drift speed in May (October), compared to July (January) for the constant wind transfer coefficient parameterizations which simply follow the peak in mean surface wind stresses. The trend in sea ice drift in this new model is +0.45 cm/s decade^{-1} compared with +0.39 cm/s decade^{-1} from the buoy observations, whereas there is essentially no trend in the standard free drift parameterization (-0.01 cm/s decade^{-1}) or the Polar Pathfinder free drifts (-0.03 cm/s decade^{-1}). The wind turning angle that minimize the cost function is equal of 25°, with a mean and root-mean square error of +2.6° and 51° on the direction of the drift, respectively. The residual from the minimization procedure (i.e. the ocean currents) resolves key large scale features such as the Beaufort Gyre and Transpolar Drift Stream, and is in good agreement with ocean state estimates from the ECCO, GLORYS and PIOMAS ice-ocean reanalyses, and geostrophic currents from dynamical ocean topography, with a root-mean-square difference of 2.4, 2.9, 2.6 and 3.8 cm/s, respectively. Finally, a repeat of the analysis on a two sub-section of the time series (pre- and post-2000) clearly shows the acceleration of the Beaufort Gyre (particularly along the Alaskan coastline) and an expansion of the gyre in the post-2000 concurrent with a thinning of the sea ice cover and observations acceleration of the ice drift speed and ocean current. This new dataset is publicly available for complementing merged observations-based sea ice drift datasets that includes satellite and buoy drift records.

1 Introduction

Communities living in Arctic regions have had an implicit understanding of the drift of sea ice for well over hundreds of years, with the sea ice playing a major role in the way of life (Aporta, 2002; Krupnik et al., 2010). Describing sea ice dynamics around

https://doi.org/10.5194/tc-2021-249
Preprint. Discussion started: 16 August 2021

Igloolik, Nunavut, Inuit elder Aipilik Inuksuk recalls: "Sometimes when there are strong winds, the new ice and the land-fast ice cannot come in contact with each other because the northerly winds cause the newly formed ice to break up and drift away. After the winds die down and the weather improves, the resultant open water freezes again and the current will move the new ice back and forth against the land-fast ice. [...] This is true, and that is the nature of the moving ice" (Inuksuk, 2011). That is to say that for a very long time, people have been aware that sea ice circulation is mainly driven by surface stresses from the atmosphere and the ocean. Over the last century, from the 1893-96 Nansen drift aboard the Fram to the 2006-07 TARA and and 2019-20 MOSAiC expeditions, polar oceanographers have tried to break down the processes relating sea ice motion to winds and oceanic currents by means of observational campaigns and theoretical development. The relationship of ice motion to external stresses is complicated by the internal rheology of the ice pack: the way in which ice resists or deforms, rather than moving when external stress is applied. In decomposing ice drift, one useful simplification is to assume that the ice is free to drift in response to the wind, i.e.: that there is no significat impact from the internal rheology. Such a free drift approximation is used in sea ice tracking models wherever the only data input is the wind field (Tschudi et al., 2019; Krumpen, 2018; Campbell et al., 2020) In this contribution, we propose a new parameterization for estimating the free drift sea ice motion, based on state variables such as thickness and concentration.

Tracking sea ice motion in the Arctic can support a wide range of studies, including to: quantify changes in the dynamic response of a thinner and less compact ice pack under climate change (Mahoney et al., 2019); investigate mechanisms for seasonal forecasting of sea ice based on late-winter off-shore ice motions, at the pan-Arctic scale or at regional scales (Nikolaeva and Sesterikov, 1970; Krumpen et al., 2013; Williams et al., 2016; Brunette et al., 2019); inform socio-environmental studies by quantifying pollutant or phytoplankton transport by sea ice between different peripheral seas (Newton et al., 2017; Lind et al., 2018) and paleoclimate studies, by identifying provenance of ice-rafted sediment to infer past sea ice drift motion and conditions (Darby, 2008; Polyak et al., 2010; Tremblay et al., 2015). Spatially and temporally complete ice motion datasets crossing the summer satellite data-desert are essential for these applications.

Free drift estimates of sea ice motion are also useful to complement other observational ice motion products. GPS-equipped drifting buoys remain the most accurate source of ice drift information, but are limited in space and time. For instance, the data record from the International Arctic Buoy Program (IABP) is composed of over 1920 buoys since 1979; but there are only a few tens to a few hundreds of buoys present at any one time. Remote sensing of the cryosphere, mainly from satellite passive microwave or synthetic aperture radar instruments, provides Arctic-wide observations of the sea ice surface, from which ice motion can be derived using different image-processing algorithms (Emery et al., 1995; Kwok et al., 1998; Meier and Dai, 2006; Lavergne et al., 2013; Tschudi et al., 2010). Reliable satellite-derived drift vectors, which are more abundant in the winter, are much more sparse in the summer, when clouds and melt-ponds affect passive microwave retrieval (Sumata et al., 2014). When neither buoy nor satellite information is available, estimates of the ice motion in response to the wind fields are essential to 'fill the gap' and maintain a spatially and temporally complete ice motion dataset, such as the National Snow and Ice Data Center's Polar Pathfinder (Tschudi et al., 2019).

Free drift is defined as the motion of sea ice in response to atmospheric and oceanic forcing in the absence of internal ice stresses. We can write the steady-state free drift $\boldsymbol{U}_i$ as a linear function of the wind velocity $\boldsymbol{U}_a$, i.e. $\boldsymbol{U}_i = \alpha \boldsymbol{U}_a + \boldsymbol{U}_w$,

https://doi.org/10.5194/tc-2021-249
Preprint. Discussion started: 16 August 2021


The Cryosphere Discussions
Open Access
EGU

where α is a wind transfer coefficient, and the residual $\boldsymbol{U}_w$ is the ocean current. α is a complex coefficient that represents the magnitude of the momentum transfer from the wind to sea ice relative to the ocean current. This wind-ice transfer coefficient includes a scaling factor $|\alpha|$, also referred to as 'wind factor' in the literature, expressed as a percentage from wind speed [m/s] to ice drift speed [cm/s], and a turning angle θ that estimates the turning angle between wind forcing and the sea ice response, due to the rotation of the Earth: $\alpha = |\alpha|e^{-i\theta}$. An estimate of this coefficient derived from the historical Fram drift gives a value of $|\alpha| \approx 2\%$ with a turning angle of $\theta = 20 - 40°$ to the right of the near-surface winds (Nansen, 1902). When considering the geostrophic wind instead, Thorndike and Colony (1982) report values of $|\alpha| = 0.8\%$ and $\theta_\alpha = 5°$ for the fall, winter and spring, and $|\alpha| = 1.1\%$ and $\theta_\alpha = 18°$ for the summer. Note that the winds veer to the left in the atmospheric boundary layer due to surface friction and the ice drifts to the right of the surface winds, leading to smaller turning angles with respect to the geostrophic wind (Leppäranta, 2011). Using geostrophic winds and buoy drift data over the 1979-1993 period, Thomas (1999) retrieved typical values for the wind-ice transfer coefficients (turning angle) of 0.7% (0°) for the winter season (defined as November-April), and 1.1% (18°) for the summer (defined as June-September). Analyzing six sea ice buoys and meteorological station 10m wind data in the Baltic Sea, Uotila (2001) reports a transfer coefficient (turning angle) in the 1.3-3.3 % (23-25°) range. Citing Thorndike and Colony (1982), the Polar Pathfinder sea ice motion dataset uses a constant wind transfer coefficient (turning angle) of 1% (20°) with surface winds from the National Centers for Environmental Prediction / National Center for Atmospheric Research (NCEP/NCAR) reanalysis (Kalnay et al., 1996).

The seasonality of Arctic surface winds is characterized by larger winds in winter compared to summer (with a maximum spanning December-January-February and minimum in May-June-July, based on the European Center for Medium-Range Weather Forecasts Atmospheric Reanalysis 5th Generation, ERA5), while the maximum sea ice drift occurs in September-October and the minimum in March. Thicker and more compact sea ice, typical of late winter conditions, results in stronger ice interactions within the ice pack, reducing the ice drift for a given wind speed, and resulting in a minimum in sea ice drift speed in the late winter, despite the winds being at their seasonal maximum (Olason and Notz, 2014; Tandon et al., 2018; Yu et al., 2020). The offset between the seasonal cycles of wind speed and ice drift speed indicates that other sea ice state parameters, are essential for describing the seasonally varying drift of ice motion. This can also be understood in terms of an energy balance for sea ice, where the power input from the surface wind stress is mainly dissipated by the water drag as well as the internal ice stresses in compact ice regions, when ice interactions are important (Bouchat and Tremblay, 2014). Mapping the distribution of the wind-ice transfer coefficient (based on passive microwave-derived ice drift and geostrophic winds over the mid-1990s), Kimura and Wakatsuchi (2000) report a sharp contrast between seasonal ice zones, such as the Bering, Barents and Okhotsk Seas, where the value can reach 2%, and the Arctic interior where the value drops to 0.8% and below; a spatial pattern which, they hypothesize, relates to stresses internal to the ice pack, and therefore to ice thickness and concentration. The same spatial pattern is observed over the 2003-2017 period by Maeda et al. (2020), who additionally report on the seasonal cycle of the wind-ice transfer coefficient (minimum around 0.8% in March and maximum around 1.1% in October), and on positive long-term trends across the whole Arctic. Interestingly, Maeda et al. (2020) note that the upward trend of the wind-ice transfer coefficient stops after 2010, particularly in regions where multi-year ice used to be prevalent. The marked differences in the seasonality of the surface wind stress and ice drift calls for a parameterization of the wind transfer coefficient that also

https://doi.org/10.5194/tc-2021-249
Preprint. Discussion started: 16 August 2021

considers ice state variables. The goal of this work is to develop such a parameterization for the wind-ice transfer coefficient (α). To the best of our knowledge, this has not been attempted before.

The proposed parameterization for the wind-ice transfer coefficient α is akin to the efforts of Steiner (2001); Lu et al. (2011); Tsamados et al. (2014); Lüpkes and Gryanik (2015), amongst others, who developed ice state dependent parameterizations for the ice-atmosphere and ice-ocean drag coefficients that are included in the momentum balance equations for numerical sea ice models. Castellani et al. (2018) demonstrate that introducing variable drag coefficients in the ice-ocean coupled configuration of the MITgcm model improves the realism of the simulation. A theoretical study by Lu et al. (2016) explores the sensitivity of the scaling factor α and the turning angle θ to variable drag coefficients dependent on ice concentration and ice floe geometry, in a free drift ice motion regime. The current study builds on the work of Lu et al. (2016) – who only considered a range of sea-ice concentration between 0-80 %, limiting the applications of their parameterization to the marginal ice zone. In contrast with these previous studies, we propose a simpler approach, in which the wind-ice transfer coefficient α is a function of the ice state, in the formulation for the free drift of sea ice. A state-dependent α can be conceptually understood as an integrated metric taking into account the spatial and temporal variability of both the atmosphere and ocean drag coefficients.

Another challenge in estimating free drift ice motion vectors arises from the poorly constrained Arctic ocean surface currents under sea ice. Existing observational approaches to estimate surface currents in the Arctic Ocean include i) the use of ocean dynamic height derived from satellite altimetry, from which geostrophic currents can be derived (Armitage et al., 2017), ii) direct current measurement from ice-tethered acoustic Doppler current profiler (ADCP, McPhee, 2013), iii) using wind stress data and depth-integrated vorticity balance (Nøst and Isachsen, 2003) and iv) deriving the mean surface ocean circulation from time-averaged sea ice drift data (Thorndike and Colony, 1982; Kimura and Wakatsuchi, 2000; Kwok et al., 2013). We expand on the approach of Thorndike and Colony (1982) for estimating the surface oceanic currents, using drifting buoys and wind data to produce updated estimates of the surface oceanic circulation in the Arctic.

One key contribution of this study is to produce a free drift product with documented errors (both spatially and temporally) that spans the shoulder season between spring and fall when satellite-based drift estimates are sparse. The hope is that this will encourage a wider range of independent seamless ice motion datasets, also covering the summer period which is oftentimes avoided because of larger error in drift estimates from passive microwave. The need for a continuous dataset for ice tracking is clear (e.g. Pfirman et al. 2004; Krumpen et al. 2016; Williams et al. 2016; Newton et al. 2017; Mahoney et al. 2019; Belter et al. 2020). Such a dataset is also included in the Sea Ice Tracking Utility, made publicly available recently on the National Snow and Ice Data Center website (SITU, Campbell et al. 2020), or the Alfred Wegener Institute ICETrack tool (Krumpen, 2018) – for educational, scientific and field expedition planning purposes.

This paper is structured as follows. Section 2 introduces the buoy, sea ice,atmospheric and oceanic datasets. Section 3 describes the methodology for parameterizing of the wind-ice transfer coefficient α. Section 4 presents the new estimates of free drift sea ice motion and quantifies the error with respect to buoy data. Section 5 summarizes the main findings presented in the paper.

https://doi.org/10.5194/tc-2021-249
Preprint. Discussion started: 16 August 2021

2 Data

2.1 Grid

We use a 25 km Equal Area Scalable Earth grid (EASE grid, Brodzik and Knowles, 2002) as a common grid for all datasets. The advantage of using the EASE grid is that all grid cells have the same area and roughly the same length in x and y. This facilitates working with vector quantities such as sea ice, ocean, or wind velocities. The u- and v-components of velocity are relative to the x- and y-directions in the EASE-grid frame of reference - i.e. they do not represent zonal and meridional velocities. All fields not natively gridded on the EASE have been interpolated to the 25km EASE grid using a Delaunay triangulation interpolation approach, which builds on piece-wise linear interpolation of scattered data.

2.2 Sea ice buoys

We use the daily buoy drift vector product included in the Polar Pathfinder dataset, distributed by the National Snow and Ice Data Centre (NSIDC, Tschudi et al. 2019). The drift vectors are calculated from the average of the offset 24-hour ice motion (midnight to midnight and noon to noon) from buoys in the IABP dataset (International Arctic Buoy Programme, 2020). In the following, we consider only buoy velocity estimates that are located within the ice edge, defined as where the sea ice concentration is higher than 15%. A total of 457,915 drift vectors are available over the 1979-2019 period, from 1920 different Arctic drifting buoys and other instruments. The drift vectors distributed by the NSIDC are stored on a 25 km EASE-grid. The estimated error on the buoy position and velocity are under 300m and 1 cm/s (Walt Myers, personal communication). In the following, we consider the ice motion vectors derived from buoy data as 'truth' when assessing the errors in the proposed free drift paramaterizations.

2.3 Polar Pathfinder free drift input data

We use the free drift ice motion input data from the Polar Pathfinder dataset as the baseline for the comparison of the proposed parameterizations. The Polar Pathfinder free drift estimates are taken as 1% of the geostrophic wind speed from the NCEP/NCAR atmospheric reanalysis (2.5° resolution), with a 20° wind turning angle. The spatial resolution of the NCEP/NCAR reanalysis is 2°. We use the daily averaged values of free drift motion vectors, stored on a 50 km EASE-grid in a checker board pattern, then interpolated to a 25 km resolution. The reported root-mean-square error on the free drift motion estimates is 6.1 cm/s from a comparison with buoys (Tschudi et al., 2019).

2.4 Surface winds

We use the 10m winds from ECMWF Atmospheric Reanalysis 5th Generation (ERA5) stored on a $1/4°$ grid (Copernicus Climate Change Service, 2017) over the 1979-2019 period. Daily mean wind velocities are calculated from hourly wind velocities. ERA5 is the reanalysis that performed best with respect to the 10m winds in a comparison of six different atmospheric reanalyses with observations from Norwegian Young Sea Ice 2015 campaign (N-ICE2015), Graham et al. (2019), with

https://doi.org/10.5194/tc-2021-249
Preprint. Discussion started: 16 August 2021

Winter/Spring/Summer correlations coefficients of 0.92/0.91/0.97, bias of +0.4/+0.1/-0.2 m/s and root-mean-square error of 1.4/1.1/0.9 m/s.

2.5 Sea ice concentration

We use the National Atmospheric and Oceanic Administration / National Snow and Ice Data Center (NOAA/NSIDC) Climate Data Record (CDR) of passive microwave sea ice concentration (Meier et al., 2017) over the 1979-2019 period, stored on a stereographic cartesian grid at a 25 x 25 km resolution. Specifically, we use the Goddard merged variable, a daily product based on the highest concentration value from either the NASA Team algorithm (Cavalieri et al., 1984) or Bootstrap algorithm (Comiso, 1986). The CDR ice concentrations have an error of 5% (Andersen et al., 2007) in the winter. In the summer, the presence of melt ponds and increased atmospheric temperatures increases the uncertainty ($\sim$10%). We use the sea ice concentration data to discriminate between motion vectors from buoys located on ice and in open water.

2.6 Sea ice thickness

Daily sea ice thickness is taken from the Pan-Arctic Ice Ocean Modeling and Assimilation System (PIOMAS) ice volume reanalysis (Zhang and Rothrock, 2003). PIOMAS is a coupled ice-ocean model, forced with atmospheric fields from the NCEP/NCAR reanalysis, and that assimilates sea ice concentration from the near real-time NSIDC product, based on the NASA Team algorithm (Lindsay and Zhang, 2006). PIOMAS correctly represents the large scale structures of ice thickness in the Arctic; while being biased thick in thin ice regions and biased thin in thick ice regions (Schweiger et al., 2011). PIOMAS data is available in near-real time for the full Arctic and year-round, and is stored on a generalized curvilinear coordinate system grid configuration with the pole shifted over Greenland.

2.7 Ocean currents

We consider four different ocean velocity products for comparison with the surface current estimates derived as a residual of the free-drift parameterization. The Estimating the Circulation and Climate of the Ocean dataset (ECCO, Fukumori et al. 2019) covers the 1992-2017 period and is based on MITgcm model runs that assimilate a suite of ocean and sea ice observations at a 1/4° resolution. We use monthly averaged values of the u-component and v-component of the ocean velocity for the topmost level (5m depth), from which we calculate the climatology. The GLORYS ocean state estimates (Mercator Ocean, 2017) runs at 1/4°, is based on a global configuration of the NEMO OGCM coupled to the Los Alamos sea ice model CICE, and assimilates observations including temperature and salinity profiles, satellite sea surface temperatures, and satellite altimetry. GLORYS is available at a daily resolution from 1993 onward. We also retrieve the oceanic currents from the PIOMAS reanalysis (Zhang and Rothrock, 2003). The PIOMAS ocean currents are produced alongside the sea ice volume reanalysis. PIOMAS daily ocean velocity vectors at a depth of 7.5 m are available over the 1979-2015 period. Lastly, we use the geostrophic ocean currents from the Centre for Polar Observation and Modelling (CPOM), which are derived from dynamic ocean topography (DOT) based on satellite altimetry (Armitage et al., 2017) - referred to as the CPOM/DOT dataset from hereon. The monthly averaged

https://doi.org/10.5194/tc-2021-249
Preprint. Discussion started: 16 August 2021

geostrophic currents are available at a 0.75° x 0.25° resolution from 2003 to 2014, covering 60°N to 81.5°N. For each of these ocean velocity products, we calculate a climatology over the common 2003-2014 period.

3 Free drift of sea ice

3.1 Momentum equation for sea ice

The conservation of momentum for sea ice can be written as (Hibler, 1979):

$$\rho_i h_i \frac{d\boldsymbol{U}_i}{dt} = \boldsymbol{\tau}_a - \boldsymbol{\tau}_w - \rho_i h_i f \hat{k} \times \boldsymbol{U}_i + \nabla \cdot \boldsymbol{\sigma} - \rho_i h_i g \nabla H_d, \tag{1}$$

where ρ_i is the ice density, h_i the ice thickness, $\boldsymbol{\tau}_a$ is the surface wind stress, $\boldsymbol{\tau}_w$ is the ocean drag, f is the Coriolis parameter, $\nabla \cdot \boldsymbol{\sigma}$ is the internal ice stresses term, g is the gravitational constant, and H_d is the sea surface dynamic height. The atmospheric stress and ocean drag are represented by quadratic drag laws:

$$\boldsymbol{\tau}_a = \rho_a C_a e^{-i\theta_a} |\boldsymbol{U}_a| \boldsymbol{U}_a, \tag{2}$$

$$\boldsymbol{\tau}_w = \rho_w C_w e^{-i\theta_w} |\boldsymbol{U_i} - \boldsymbol{U_w}| (\boldsymbol{U_i} - \boldsymbol{U_w}), \tag{3}$$

where ρ_a and ρ_w are the air and water densities, C_a and C_w are the air-ice and ice-water drag coefficients, θ_a and θ_w are the air and water turning angles, $\boldsymbol{U_a}$ is the 10m wind vector and $\boldsymbol{U_w}$ is the geostrophic ocean current vector. The ice velocity is neglected in the surface air-ice stress (Eq. 2) because $\boldsymbol{U_i}$ is typically much smaller than $\boldsymbol{U_a}$. Assuming steady-state, thin ice and neglecting internal ice stress, the main balance of terms in the momentum equation become: $\boldsymbol{\tau_a} = \boldsymbol{\tau_w}$, or:

$$\rho_a C_a e^{-i\theta_a} |\boldsymbol{U}_a| \boldsymbol{U}_a = \rho_w C_w e^{-i\theta_w} |\boldsymbol{U}_i^{fd} - \boldsymbol{U}_w| \ (\boldsymbol{U}_i^{fd} - \boldsymbol{U}_w), \tag{4}$$

where $\boldsymbol{U}_i^{fd}$ is the free drift ice velocity. In this simple case, an analytical solution for the ice velocity can be written as a function of the wind and ocean current velocities and a wind-ice transfer coefficient (α) (Leppäranta (2011)):

$$\boldsymbol{U}_i^{fd} = \alpha e^{-i\theta} \boldsymbol{U}_a + \boldsymbol{U}_w, \tag{5}$$

where θ is an integrated turning angle that takes into account the turning in the surface ocean Ekman layer and (indirectly) the Coriolis effect, and where

$$\alpha = \sqrt{\frac{\rho_a C_a}{\rho_w C_w}}. \tag{6}$$

This simple relation explains roughly 70% of the variability in sea ice velocity in the central Arctic (Thorndike and Colony, 1982). Exceptions include low wind speeds or thick ice when the Coriolis effect is more important (drag scales with ice velocity square and Coriolis scales with thickness) and non-negligible internal ice stresses (Thorndike and Colony, 1982; Bouchat and Tremblay, 2014).

https://doi.org/10.5194/tc-2021-249
Preprint. Discussion started: 16 August 2021


The Cryosphere Discussions

3.2 Minimization procedure

We use a least squares minimization approach to find the coefficients (α, θ) and ocean currents ($\boldsymbol{U}_w$) that will minimize the error function:

$$E_{(\alpha,\theta)} = \sum_{k=1}^{n} [\boldsymbol{U}_{buoy}^{k} - \boldsymbol{U}_{i}^{fd}(\alpha,\theta)^{k}]^2 \tag{7}$$

where n is the total number of observational points, $\boldsymbol{U}_{buoy}$ are the buoy drift observations, and the free drift velocities $\boldsymbol{U}_{i}^{fd}$ are estimated at the same locations and times as the buoy observations. Note that α, can be either a constant or parameterized as a function of sea ice state variables (h_i and A). We solve the minimization problem using the Levenberg-Marquardt lest-squares algorithm (MATLAB *lsqcurvefit* function). The error function is first differentiated with respect to each of the free parameters, and the resulting system of linear equations is solved iteratively using a combination of Gauss-Newton and steepest descent methods. Note that the minimization procedure minimizes the cost function based on the u- and v-components of the drift. One consequence of this is that there can be a residual rms error on the speed (a nonlinear function of u and v, see discussion below). In a first step, the $\boldsymbol{U}_w$'s are considered known, and we find the free parameter(s) for α that minimizes the error function. In a second step, the wind transfer coefficient(s) is (are) considered known and we solve for the time-constant but spatially varying ocean currents $\boldsymbol{U}_w$. This iterative procedure is repeated until convergence. Assuming that the component of ice motion that is not explained by the winds can be attributed to ice-ocean drag, we assign the residual of the linear regression of the free drift transfer function, or the y-intercept in the best linear fit, to the ocean current vectors, as defined in Thorndike and Colony (1982).

The full convergence of the solution is reached within 5 iterations. Using this iterative procedure reduces the size of the matrix passed to the least-squares solver, and therefore greatly reduces the memory requirement. The initial guess for the iterative procedure is a value of one (unit-value) for all free parameters. The final solution (i.e. the minimum in the error function) is independent of the initial guess and the resulting wind-ice transfer coefficients ranges from 1-2.5% (in line with previous estimates) depending on whether α is constant or sea ice state dependent.

The density of the data is such that there is insufficient information for interannually-varying ocean current fields. Therefore, we created a single climatology (40-year mean) ocean current field. In the evaluation of the ocean currents, we use the 3x3 grid-cell mean (75 km x 75 km) centered on the target grid cell i, j to have enough data points for the minimization procedure (Fig. 1). The size of this search window was defined such that at least 10 data points are present for each of the grid cell in the domain. This also allows for an estimate of the ocean current at each grid cell of the pan-Arctic domain (with the exception of parts of the Eurasian plateau where buoy data is not included in the IABP dataset). The averaging introduces a smoothing of surface current features over a scale of 75 km and allows for the representation of large-scale features such as the Beaufort Gyre and Transpolar Drift Stream. This is not considered an issue in the contest of long time-averaged fields.

https://doi.org/10.5194/tc-2021-249
Preprint. Discussion started: 16 August 2021

Table 1. Values obtained from a least squares fit using buoy data (IABP), 10m wind velocity (ERA5) and ice thickness (PIOMAS) over the 1979-2019 period. These parameterizations include the free drift used in the Polar Pathfinder dataset (α_p), a bias corrected constant wind-ice transfer coefficient ignoring the ocean currents (α_0) and considering nonzero ocean currents (α_w), and a thickness-dependent free drift (α_h). The five rightmost columns present the root-mean-square error (RMSE) and mean bias error on drift speed, u- and v-components, and drift angle, and the explained variance (R^2), evaluated at the IABP buoy data location.

		Coefficients			Error metrics: **RMSE** (Mean bias error)				
Name	Parameterization	α [%]	β [1/m]	θ [°]	$\lvert \boldsymbol{U}_i \rvert$ [cm/s]	u_i [cm/s]	v_i [cm/s]	θ [°]	R^2
α_p	$\alpha_p e^{-i\theta_p}$	1.0	-	20	**7.4** (-3.8)	**5.7** (0.2)	**5.7** (-1.1)	**54** (-6.9)	0.35
α_0	$\alpha_0 e^{-i\theta_0}$	1.4	-	23	**6.2** (-0.8)	**5.3** (0.0)	**5.1** (0.0)	**55** (2.3)	0.33
α_w	$\alpha_w e^{-i\theta_w}$	1.3	-	24	**5.4** (-0.5)	**4.8** (0.0)	**4.6** (0.0)	**51** (2.6)	0.48
$\alpha(h)$	$\alpha_h(1-\beta_h h_i)e^{-i\theta_h}$	2.0	0.17	25	**5.1** (-0.5)	**4.6** (0.0)	**4.2** (0.0)	**51** (2.6)	0.55

4 Results and discussion

Our goal is to derive a free drift parameterization that is bias-corrected with respect to the buoy drift data from IABP - and that is sea ice state-dependent in order to take into account the seasonality and long-term trends in the sea ice drift. This seasonality is directly related to seasonal changes in sea ice thickness. The long-term changes in sea ice thickness associated with global warming are of the same order of magnitude as the seasonal change (Rothrock et al., 2008; Rampal et al., 2009), which implies that there will be a trend in α from the parameterization as well. For clarity, we use subscripts for denoting the wind-ice transfer coefficients and wind turning angle in the different parameterizations of free drift:

- α_p, θ_p: Polar Pathfinder parameterization (referred to as "standard" in the following Thorndike and Colony, 1982);
- α_0, θ_0: constant wind-ice transfer coefficient, no ocean currents;
- α_w, θ_w: constant wind-ice transfer coefficient, including ocean currents;
- α_h, θ_h: thickness-dependent parameterization;

as well as an additional free parameter β_h for the thickness parameterization (see explanation below).

4.1 Bias-corrected free drift

In the following, we use the constant Polar Pathfinder parameterization as our reference to which other parameterizations are compared. We first consider the standard free drift parameterization, (Thorndike and Colony, 1982; Tschudi et al., 2019), for which the root-mean-square error (mean bias error) on the total speed, u- and v- components is 7.4 (-3.8), 5.7 (0.2) and 5.7 (-1.1) cm/s, respectively. The bias-corrected free drift parameterization (α_0) with a constant wind transfer coefficient and no ocean currents – one that minimize the error function above (Eq. 7), as opposed to a fixed 1% and 20° α and θ – reduces

https://doi.org/10.5194/tc-2021-249
Preprint. Discussion started: 16 August 2021

the root-mean-square error and mean bias error by 16% (6.2 vs 7.4 cm/s) and 79% (3.8 vs -0.8 cm/s) when compared to all observed sea ice drift from buoy data (see Fig. 2). Note that the residual bias in the speed is non-zero since the minimization is done on the u- and v-components and speed is a non-linear function of u and v. When considering non-zero ocean currents (α_0), the root-mean-square error and mean bias error are reduced by 13% (from 6.2 to 5.4 cm/s) and 40% (from -0.8 to -0.5 cm/s). This result is in agreement with a single-drifter analysis of Uotila (2001), where the addition of ocean currents along a buoy track reduces by 18% the mean velocity difference between simulated and observed velocities. Regarding the error on the drift direction, the bias-corrected α_w reduces root-mean-square and mean bias error compared to the standard parameterization α_p, by 6% ($54°to51°$) and 62% ($-6.9°to+2.6°$), where a positive value in mean bias error indicates that the drift estimate is to the right of the buoy drift (Fig. 3h,i). We note that, for the bias-corrected α_w parameterization, over the 1979-2018 period, the use of the 1/4° ERA5 reanalysis over the 1° ERA-Interim reanalysis for the 10m wind speed reduces the root-mean-square error on the drift speed (and directional error) from 5.7 cm/s (56°) to 5.4 cm/s (51°) [results not shown]. To summarize this first step: we observe a reduction of the error and bias on the drift speed by 1.2 cm/s and 3 cm/sec by minimizing a cost function for the wind-ice transfer coefficient and angle, and by using a higher spatial resolution atmospheric reanalysis (ERA5); and a further reduction of the error by 0.8 cm/s taking into account the ocean current as the residual of the linear fit between the surface wind stress and ice drift speed.

The error reduction can be clearly seen in the distribution of ice drift speed (Figure 3e,f), where the constant wind-ice transfer parameterization α_w yields a distribution that is in better agreement with that of the buoys, compared to the standard parameterization α_p. A peak at zero velocity is present in the buoy drift speed distribution, due to the presence of landfast ice or thicker ice north of the Canadian Arctic Archipelago, a feature which none of the free drift parameterizations is expected to reproduce. The constant parameterization including ocean currents α_w also contributes to reducing the relative error (defined as the root-mean-square error divided by the mean). The bias-corrected α_w parameterization reduces the seasonal relative error by 23% and the interannual relative error by 22% compared to the standard α_p parameterization (Fig. 5c,d). However, the α_w parameterization does not improve the explained variance of the interannual variability of the drift speed (Fig. 5b): the R^2 (adjusted R^2) is 0.28 (0.26) for α_p, and 0.23 (0.21) for the α_w parameterization, which is expected since α_w does not take into account the variability of the sea ice state. The interannual variability of sea ice drift speed based on buoy data can result from variability in the atmospheric forcing, oceanic forcing, and sea ice state as well as from the uneven spatial sampling of the buoy data. However, Rampal et al. (2009) investigated the trends in sea ice motion based on the IABP data, and ruled out the influence of spatial sampling of the buoys on their results.

Surprisingly, taking sea ice concentration into account to estimate the seasonally-varying transfer coefficient does not improve the agreement between drift estimates and observations, even when compared to a constant wind-ice transfer coefficient (see Appendix). This dependency, which we presume exists, may not be picked up in our minimization procedure because most of the buoy data are located in high ice concentration areas (85% of the buoy data points are in sea ice of concentration >95%). Almost no data come from buoys located along the Eurasian coastline where free drift and a looser pack ice is present, particularly in the summer.

https://doi.org/10.5194/tc-2021-249
Preprint. Discussion started: 16 August 2021


The Cryosphere Discussions
Open Access
EGU

4.2 State-dependent wind-ice transfer coefficient

Next, we note the striking similarity between the spatial distribution of climatological sea ice thickness in the Arctic Ocean (Laxon et al., 2013) and the observed spatial distribution of the wind-ice transfer coefficient derived from the IABP buoy drift and ERA5 wind reanalysis data (Fig. 4a,b). The α coefficients are in the 0-2.5 % range, in line with previous estimates of the scale and spatial variability of the wind-ice transfer coefficient by Thomas (1999) based on buoy data and geostrophic winds. They agree as well with spatial fields of α estimated by Kimura and Wakatsuchi (2000) and Maeda et al. (2020), who build on the ratio of satellite-derived ice drift speed over geostrophic wind speed. The corresponding mean and standard deviation of the drag coefficient ratio (C_a/C_w) - the key parameter governing the magnitude of the sea ice drift (McPhee, 1980; Harder and Fischer, 1999), - are 0.19 and 0.11, respectively, for $\rho_a = 1.3$ kg/m^3 and $\rho_w = 1026$ kg/m^3 (Fig. 4d). These agree with typical values used in the Arctic sea ice modeling community and derived from observations (0.22, Hibler 1979; 0.19, Leppäranta 2011; 0.2-0.25, Lu et al. 2016).

The results from this simple analysis suggest a linear dependence of the wind transfer coefficient on sea ice thickness, i.e.:

$$\alpha(h) = \alpha_h(1 - \beta_h h_i)e^{-i\theta_h}, \tag{8}$$

where α_h is the maximum value of the transfer coefficient for the free drift regime, β_h is an ice-thickness (h_i) parameter modulating $\alpha(h)$, and θ_h is the wind-ice turning angle for the thickness-dependent parameterization. The error minimization routine yields an α_h coefficient of 2.0%, and the net wind-ice transfer term decreases linearly until sea ice reaches a thickness of 6.1 m (after which it is floored to zero). Using the thickness-dependent transfer coefficient $\alpha(h)$, the root-mean-square error (mean bias error) for the u- and v-components of the velocity, and for the total ice drift speed are respectively $4.6\ (1 \times 10^{-2})$ cm/s, $4.2\ (4 \times 10^{-3})$ cm/s and $5.1\ (-0.5)$ cm/s. This represents an additional improvement on the root-mean-square error of 6% (5.1 vs 5.4 cm/s) compared to the constant parameterization α_w (the mean bias error is unchanged). With respect to the standard α_p parameterization, this represents a total reduction of the error and mean bias error of 31% (5.1 vs 5.4 cm/s) and 86% (-0.5 vs -3.8 cm/s). Using a similar linear free drift model built on monthly-fitted values of the wind-ice transfer coefficient and turning angle over the 1983-1987 period, Thomas (1999) obtain a root-mean-square error of 5.2 cm/s for entire Arctic Ocean. The similarity of the best fit error from two different time periods causes us to speculate whether ca. 5 cm/s might constitute a lower limit to the accuracy of free drift estimates from linear minimization, with free parameters.

The benefits of a thickness dependent parameterization $\alpha(h)$ emerges when we consider the seasonal cycle and interannual variability of sea ice drift speed (Fig. 5). Both the standard α_p and bias-corrected α_w parameterizations follow the seasonality of the wind speed (Fig. 5a). Including a thickness dependence improves the representation of the seasonal cycle of sea ice drift speed as observed in the buoy data, by better capturing the peak of ice drift speed in October and by shifting the drift speed minimum from July to May. Free drift estimates are most heavily used in the summer, when less satellite-derived ice motion estimates are available, which highlights the importance of including time-dependent sea ice state variables in the estimation scheme. The $\alpha(h)$ thickness-dependent parameterization reduces the seasonal relative error by an additional 2% on average compared to the constant α_w parameterization (which amounts to a 28% average reduction of the seasonal relative error compared to the standard α_p). The relative error is lowest in the summer ($\sim$0.75) and peaks in the winter ($\sim$1). Highest

https://doi.org/10.5194/tc-2021-249
Preprint. Discussion started: 16 August 2021

relative errors are expected in the winter, since the ice speed is at a seasonal minimum, and the root-mean-square error is maximal due to wintertime ice interactions not being represented by a free drift model.

The time series of annually averaged sea ice drift speed (calculated from the estimates at buoy locations) also reveals that the thickness-dependence – $\alpha(h)$ – contributes to capturing long-term trends in sea ice drift speed (Figure 5b). The constant α_w parameterization results in virtually no trend on the ice drift speed (-0.01 cm/s decade^{-1}, not significant), so does the standard α_p parameterization (-0.03 cm/s decade^{-1}, not significant), whereas the thickness dependent $\alpha(h)$ parameterization yields a trend (+0.45 cm/s decade^{-1}) that is much closer to what is observed from the buoy data (+0.39 cm/s decade^{-1}). Constant α_w ice motion results in an overestimate of the buoy drift speed in the earlier part of the record, and an underestimate it in the later part of the record. This indicates that the climatological thinning of sea ice is key in driving the long term trend in ice drift speed in the Arctic, supporting the findings of Rampal et al. (2009) and Kwok et al. (2013), who respectively use buoy and satellite-derived ice motion to attribute the trend in ice drift speed to the thinning of sea ice and to the loss of multiyear ice. In addition, the new free drift estimates capture a majority of the interannual variability of annually averaged ice drift speed ($R^2 = 0.76$), which is largely missed in the standard free drift parameterization α_p ($R^2 = 0.28$). An additional feature of the time series of the annual relative error is that all the parameterizations show a similar pattern: the relative error is lower in the earlier part of the record and then slowly increases after the 2000s. This could be linked to increasing drift speed, which is also generally prone to a larger absolute error. Nevertheless, the $\alpha(h)$ parameterization remains the best free drift parameterization presented herein, having the lowest relative error in the later part of the record (Figure 5c).

The relative error (root-mean-square error divided by mean) is highest (>1) along coastlines and in regions of thicker ice (north of the Canadian Archipelago), and progressively decreases towards the central Arctic Ocean (Figure 6). The relative error is minimal ($\sim$0.4) along the Transpolar Drift Stream and along the East Greenland Current, south of Fram Strait. This can be understood as an indicator of the quality of the thickness-dependent linear free drift estimates for representing different regions and ice motion regimes. Along the Transpolar Drift Stream, in the absence of confining pressure to the south, since Barents Sea is open, internal ice stresses are minimal and the free drift regime offers a good description of the motion field. On the other hand, in the Canadian Arctic Archipelago, or along the Alaskan coastlines or Eurasian coastlines, effects such as landfast ice and internal stresses under onshore winds limit free drift. Then Equation 5 is a poor approximation, and the linear free drift estimates lose their fidelity. In addition, ice motion vectors from satellite imagery are often unavailable due to land contamination of the pixel, which leads a number of data providers not to provide ice motion estimates in the exact vicinity of the coast within, e.g., 25km of the coasts for the Polar Pathfinder merged dataset (Tschudi et al., 2019). Finally, the representation of free drift in Equation 5 is isotropic, making it inadequate fro the treatment of coastlines. Attempts have been made at constructing an anisotropic response using vector regressional analysis (Rabinovich et al., 2007) to better represent coastal interactions, but this is beyond the scope of the present study.

The $\alpha(h)$ parameterization does not further improve the directional root-mean-square error (mean bias error), which is $51°$ ($+2.6°$), which is the same as the constant α_w parameterization (Fig. 3g). This is expected as the θ turning angle parameter itself is constant, i.e. not parameterized as a function of ice thickness. Interestingly, Togunov et al. (2020) report very similar numbers: compared to drifting telemetry collars in the Hudson Bay, the Polar Pathfinder ice motion (essentially based on free

https://doi.org/10.5194/tc-2021-249
Preprint. Discussion started: 16 August 2021

drift estimates in that region) yields an average drift direction error of $2.6° \pm 53.9°$. We also note a dependence of the directional error on the ice drift speed (Fig. 7). The drift direction is inaccurate for low values of buoy drift speed, but the spread of the error reduces and centers around zero with increasing sea ice drift speeds. Low directional errors for higher ice drift speed is also reported in other studies that compare Polar Pathfinder ice motion vectors to drifting telemetry collars (Togunov et al., 2020) and that compare passive microwave sea ice drift to ice-tethered profilers (Hwang, 2013). This result is expected, as several instances of low sea ice drift speed - when not driven by low winds - are the results of important ice-ice interactions. Since internal ice stresses are not considered in the free drift momentum balance, the direction of free drift estimates over regions subject to coastal effects or populated with thick, compact ice can easily diverge from buoy observations. Looking forward, the inclusion of a variable wind turning angle should be considered for improving the accuracy of free drift ice motion estimates. A simple attempt at representing the dependence of the drift angle on sea ice thickness by a linear relationship was tested (see Appendix), but did not contribute to reducing the error on the drift direction. Leppäranta 2011 (eq. 6.7b) do a formal derivation for wind-ice turning angle in a free drift regime, showing that it is a function of Coriolis forcing divided by the ocean drag. While this might help reduce the error, the introduction of the ice drift speed in the parameterization of the wind-ice turning angle removes the elegance of the simple linear free drift parameterization. Other interesting approaches include Hongwei et al. (2020) and Park and Stewart (2016) who observe a cubic polynomial relationship between the wind turning angle and 10m wind speed, based on ice-tethered buoys deployed in the central Arctic in 2012. Future work will include testing parameterizations for the wind-turning angle in free drift models.

4.3 Surface ocean current estimates

A caveat of our approach is the use of a fixed ocean current climatology to calculate the ice motion estimates. The variations of the sea ice drift speed have a significant seasonal signature on top of a long-term trend (Fig. 5a,b); and due to a strong coupling of the ice-ocean system in the Arctic, these variations of ice drift speed also drive variations of the surface currents. As explored by Meneghello et al. (2018) in model studies, the slowdown of the ice speed in the winter can lead to an inversion of the surface ice-ocean stresses; modulating the surface currents seasonally. With respect to the long-term trends, Armitage et al. (2017) report increased oceanic surface current speeds over the 2003-2014 period, concurrent with a thinner, weaker and looser sea ice cover. The inclusion of these two features of the oceanic currents variability in our free drift parameterization would help improve the representation of the seasonal cycle and the long-term trends in ice drift speed.

The under-ice ocean current estimates obtained from the error minimization procedure capture the general features of the oceanic surface circulation in the Arctic, clearly showing the Beaufort Gyre and the Transpolar Drift Stream (Figure 8a). The speeds of surface currents are approximately 70% of the long-term, time-averaged sea ice drift speed, in general agreement with the assumption made by Thorndike and Colony (1982) who provided early estimates of the mean Arctic ocean circulation from ice drift velocity based on buoy data. The currents are slower north of the Canadian Archipelago, and faster in the southern branch of the Beaufort Gyre and along the coast of Greenland. The currents speeds follows a Rayleigh distribution, and have a mean of 3.5 cm/s. These results are qualitatively similar to those of Kimura and Wakatsuchi (2000), based on different

https://doi.org/10.5194/tc-2021-249
Preprint. Discussion started: 16 August 2021

reference periods), who make estimates of the current by subtracting the time-averaged passive-microwave ice motion from time-averaged geostrophic winds.

We produce estimates of the surface currents before and after 2000 when a change in the trend in the minimum sea ice extent record occurred (Figure 9a and 9b). Although the number of observations is uneven (130,146 and 327,769 data points in the earlier and later part, respectively), they are sufficient to reconstruct climatological surface current estimates. Results indicate a distribution in sea ice drift speed that is higher for the later part of the record (see Fig 9c), consistent with the positive trend in sea ice drift speed reported by Rampal et al. (2009). The associated increase in current speed is most apparent along the southern branch of the Beaufort Gyre, from the Alaskan coastlines to the center of the Chukchi sea. A striking feature of the pre/post 2000s oceanic circulation is the expansion of a branch of the Beaufort Gyre over the Northwind Ridge and the Chukchi plateau. These findings are in line with Armitage et al. (2017) and Regan et al. (2019) who report an acceleration of the currents in the southwestern Beaufort Sea and a north-westward expansion of the Gyre, based on geostrophic currents derived from satellite radar altimetry. An intensification of the geostrophic currents in the periphery of the Gyre is also seen in hydrographic data obtained over the 2003-2011 period from ice-tethered profilers and shipboard surveys (McPhee, 2013). The expansion of the Beaufort Gyre over the Chukchi plateau is also found in models, and its dynamics are investigated in more details in Regan et al. (2020). These findings are coherent with a trend towards more open water in the summer season as well as faster ice drift due to thinner (Fig. 9e) and less compact ice, which in turn entrains the ocean surface layer, while no large-scale acceleration of the wind speed is found (Fig. 9f). We also relate these results to the increase in freshwater content in the Beaufort Gyre, which trends and interannual variations are well documented by Proshutinsky et al. (2019). Comparing trends in the wind field curl and sea surface height in the Beaufort Sea (from which the doming of the gyre can be assessed, hence the accumulation in freshwater), Giles et al. (2012) conclude that the transfer of momentum from the atmosphere to the ocean increased at the turn of the 2000s. Similarly, McPhee (2013) use hydrographic data and note the increased doming of the gyre over the 2003-2011 period, marked by larger downward Ekman pumping at the center, and steeper gradients and faster geostrophic currents on the periphery of the gyre. Our findings of faster currents in the Beaufort Gyre, coinciding with a reduction in ice thickness, support these conclusions and highlight the contribution of dynamic processes to the freshening of the gyre. The impacts of the declining ice draft to the freshwater cycle in the Beaufort Gyre are explored in more details in Krishfield et al. (2014). Based on mooring and satellite altimetry data, they note the decrease in multiyear ice and its replacement by thin ice or open water, which caused a reduction of the solid fresh water volume in thegyre, and an increased contribution of liquid water to the accumulation of freshwater. Krishfield et al. (2014) observe a stabilization of the freshwater content in the Beaufort Gyre in recent years. In a recent study, Armitage et al. (2020) explain the stabilization freshwater content by increasing eddy energy dissipation; as the currents speed up, this implies a more energetic Arctic Ocean.

Additionally, we present estimates of the ocean currents $\boldsymbol{U}_w$ for the high and low sea ice drift speed seasons, respectively defined as July to December, and January to June. We refer to these as the 'summer' and 'winter' seasons, from the sea ice drift point of view. The currents tend to be faster in the summer, specifically in the Southern branch of the Beaufort Gyre, consistent with a seasonal reduction in ice thickness (Figure 10c,e). We also note that the surface currents in Fram Strait and east of Greenland appear to be slightly slower in the summer, potentially explained by the minimum in the wind speed seasonal cycle.

https://doi.org/10.5194/tc-2021-249
Preprint. Discussion started: 16 August 2021

Interestingly, the general winter/summer contrast in estimated ocean currents speed resembles the pre/post-2000s difference, which in both cases can be related to differences in ice thickness. The long term trend in sea ice thickness reduction affects the ice-ocean system in a way that is analogous the seasonal cycle: the presence of perennial ice in the pre-2000s was favorable to drift conditions that were similar the winter climatology, whereas the modern transition towards a seasonal pack ice constitutes an ice-ocean system that resembles the summer climatology.

Our buoy-derived surface currents can be used as an independent source of comparison for different oceanic state estimates from observations or reanalyses (Figure 11). We calculate the climatology of buoy-derived ocean currents over the 2003-2014 period for different Arctic ocean state products: ECCO (Fukumori et al., 2019), GLORYS (Mercator Ocean, 2017), PIOMAS (Zhang and Rothrock, 2003) and the CPOM/DOT geostrophic currents derived from the dynamical ocean topography (Armitage et al., 2017). The climatologies from ECCO, GLORYS, PIOMAS and CPOM/DOT yield the expected features of surface Arctic oceanic circulation, with the GLORYS and PIOMAS reanalyses showing marginally faster current speeds than the other products. Our estimates are generally in good agreement with the other ocean velocity products, the pan-Arctic root-mean-square difference (and relative difference, defined as root-mean-square difference divided by the mean of each product) between our climatology and ECCO, GLORYS, PIOMAS and CPOM/DOT are respectively 2.4, 2.9, 2.6 and 3.8 cm/s (0.82, 0.83, 0.76 and 1.30). For the central Arctic, the difference in current speed is only $\pm$ 1 cm/s. A common pattern emerges: our sea ice buoy-derived estimates tend to be slightly slower north of the Canadian Archipelago and along the Alaskan coast, and faster north of Fram Strait and along the East Greenland current. The low speed bias may be due to a misreprentation of the internal ice stress in models. The largest differences are located in the East Greenland current where our estimates are over 5 cm/s faster than all of the other ocean velocity products. When comparing to PIOMAS specifically, we note faster currents in the southern Beaufort Sea, and slower currents in the interior of the Beaufort Gyre. A misplaced center of action of the Beaufort Gyre could reasonably explain this pattern. We also note two regions, along the coastlines of the Canadian Archipelago and along the Alaskan North Slope, where GLORYS is significantly faster than our estimates of the currents. Since ice speed in GLORYS is from a model that drives the surface ocean, we hypothesize that the low speed bias in these specific regions can relate to an imperfect rheological model, on which relies the ice-ocean momentum transfer where ice interactions are large. The work required to dissect these differences in ocean current speed, however this is beyond the scope of the present study. Nevertheless, when considering the larger picture, the good agreement between our estimates of ocean currents in the central Arctic and the observations-based CPOM/DOT data, and the general similarities between our climatology and ECCO, GLORYS, PIOMAS indicate that the reanalyses capture reasonably well the general ocean circulation in the central Arctic.

5 Conclusions

Wind-driven ice motion estimates are an essential component of merged ice motion datasets (e.g.: Polar Pathfinder, Tschudi et al., 2019), providing information on sea ice drift when neither buoys nor satellite-derived drift vectors are available. In this study, we present new estimates of sea ice motion based on the free drift of sea ice, introducing a sea ice state dependent wind-ice transfer coefficient. Free drift is defined as the response of sea ice to the wind and ocean stresses, in the absence of internal

https://doi.org/10.5194/tc-2021-249
Preprint. Discussion started: 16 August 2021

ice stresses, which is described by: $\boldsymbol{U}_i = \alpha \boldsymbol{U}_a + \boldsymbol{U}_w$ (Thorndike and Colony, 1982; Leppäranta, 2011). This established linear relationship between sea ice velocity ($\boldsymbol{U}_i$), wind velocity ($\boldsymbol{U}_a$) and surface ocean currents ($\boldsymbol{U}_w$), where α is the wind-ice transfer coefficient. Using a 40-year record (1979-2019) of buoy data from the International Arctic Buoy Program and 10m wind velocity from the ERA5 reanalysis, we find a spatial dependence of the wind-ice transfer coefficient on sea ice thickness (h_i) similar to that of the simulated (PIOMAS) or observed sea ice thickness distributions. The wind-ice transfer coefficient is lowest in regions populated with thick ice (e.g.: north of the Canadian Arctic Archipelago) and the transfer coefficient increases in the peripheral Arctic seas which are seasonally covered with much thinner sea ice. The spatial pattern of wind-ice transfer coefficient is consistent with Maeda et al. (2020), increasing our confidence in the results. Based on these results, we parameterize the wind-ice transfer coefficient as a linear function of sea ice thickness such that: $\alpha(h) = \alpha_h(1 - \beta h_i)e^{-i\theta_h}$, where α_h and β are free parameters controlling the amplitude of the wind-ice transfer coefficient, and θ_h is a wind turning angle that accounts for the Coriolis effect. We use a least-squares minimization approach and obtain the following values for the free parameters: $\alpha_h = 2.0\%$; $\beta = 0.17$ m^{-1} and $\theta_h = 25°$.

We use the thickness-dependent free drift parameterization $\alpha(h)$ to produce ice motion estimates which we compare to the 40-year record of buoy drift. The free drift estimates yield root-mean-square errors (mean bias error) of 5.1 cm/s (-0.5 cm/s) for the drift speed and 51° (2.6°) for the drift direction. This represents a 31% reduction of the error on the ice drift speed compared to the free drift estimates presently used in the Polar Pathfinder dataset. One of the key advantages of the thickness-dependent free drift is a better representation of the seasonal cycle and interannual variability of sea ice drift speed. Including a dependence on ice thickness shifts the seasonal cycle of ice motion estimates towards observations. The seasonal cycle of the error is also characterized by a minimum relative error in the summer period (July-October), which is a desirable feature since free drift estimates are mostly used in the summer season when a lesser number of ice motion vectors from satellites are available.

In the proposed minimization procedure, the ocean currents appear as a residual (i.e. assumed to be part of the signal in sea ice drift speed that is not explained by surface winds) Thorndike and Colony 1982). The climatology of these surface ocean current estimates captures the general features of the Arctic Ocean general circulation, including the Beaufort Gyre, the Transpolar Drift Stream, and a fast outflow current along the eastern coast of Greenland. We explore climatological changes in the ocean state by retrieving the ocean currents for the pre- and post-2000s periods. We observe a general acceleration of the surface currents, concurrent with a reduction in sea ice thickness from the pre-2000s to the post-200s. The most striking feature of the climatological changes in the ocean state is a sharp acceleration of the southern Branch of the Beaufort Gyre and an expansion of the Gyre over the Chukchi Rise, a feature also reported in other studies using different methods (McPhee, 2013; Armitage et al., 2017). Our approach provides independent estimates of the surface ocean currents under sea ice, that can be used in conjunction with observations of the currents from altimetry or ice-tethered profilers for improving our understanding of the Arctic Ocean circulation.

Future work includes the development of an optimal interpolation approach for integrating our free drift estimates to other ice motion inputs provided as part of the Polar Pathfinder dataset; and performing an intercomparison of different Arctic ocean state estimates and our independent climatology of the surface ocean currents.

https://doi.org/10.5194/tc-2021-249
Preprint. Discussion started: 16 August 2021

The Cryosphere Discussions
Open Access
EGU

Table A1. List of additional free drift parameterizations tested in the context of this study. The error metrics are based on a comparison to the IABP buoy sea ice drift data over 1979-2019.

		Coefficients			Error metrics: **RMSE** (Mean bias error)					
Name	Parameterization	α	β	C	θ [°]	$\lvert\boldsymbol{U}_i\rvert$ [cm/s]	u_i [cm/s]	v_i [cm/s]	θ [°]	R^2
$\alpha(A)$	$[\alpha_A - (\alpha_A - \beta_A)e^{-C(1-A)})]e^{-i\theta_A}$	1.6	1.2	35.6	24	**5.5** (-0.5)	**4.9** (0.0)	**4.4** (0.0)	**52** (2.8)	0.49
$\alpha(A,h)$	$[\alpha_{Ah} - (\alpha_{Ah} - \beta_{Ah})h_i e^{-C(1-A)})]e^{-i\theta_A}$	2.0	1.7	0.41	24	**5.2** (-0.5)	**4.7** (0.0)	**4.3** (0.0)	**52** (2.8)	0.54
$\theta(h)$	$\alpha_\theta e^{-i\theta_h(1+\beta_h h_i)}$	1.3	-0.069	-	28	**5.4** (-0.4)	**4.9** (0.0)	**4.5** (0.0)	**52** (8.4)	0.48

Code and data availability. Code and data are available at https://web.meteo.mcgill.ca/~charles/freedrift/

Appendix A: Other formulations

A number of different, equally intuitive, parameterizations were also tested, yet they did not reduce the root-mean-square error with respect to the buoy data (Table A1). We report on them here to inform others interested in similar questions. In fact, the parameterization based on ice thickness alone is the simplest and provides the lowest root-mean-square error. Following Hibler 1979, we first tested a wind transfer coefficient with an exponential decay with sea ice concentration variations:

$$\alpha(A) = \alpha_A - (\alpha_A - \beta_A)e^{-C(1-A)}. \tag{A1}$$

The three free parameters α_A, β_A and C represent the free drift wind transfer coefficient, the fully ice-covered wind transfer coefficient, and a decay coefficient between free drift and full ice cover. Secondly, we tested a wind transfer coefficient that has a dependence on both sea ice concentration and thickness:

$$\alpha(A,h) = \alpha_{Ah} - (\alpha_{Ah} - \beta_{Ah})h_i e^{-C(1-A)}, \tag{A2}$$

where the free parameters have the same meaning as for the previous equation.

Lastly, we tested a thickness-dependent wind turning angle, to account for the fact that the deviation from the surface wind will be larger for thicker ice because of the linear dependence of the Coriolis parameter on ice thickness:

$$\alpha_\theta e^{-i\theta_h(1+\beta_h h_i)} \tag{A3}$$

None of the above formulations lead to an improved parameterization of the drift velocity and angle. The root-mean-square error on the $\alpha(A,h)$ parameterization is similar to that of the $\alpha(h)$ parameterization based on ice thickness alone, indicating that the predictive skill all lies in the knowledge of the thickness field.

https://doi.org/10.5194/tc-2021-249
Preprint. Discussion started: 16 August 2021

Author contributions. CB and BT designed the study and prepared the manuscript. RN and BT conducted preliminary data collection and analysis. CB and BT conducted the present version of the study. CB retrieved the data, developed the code and prepared the figures. All authors collaborated in editing the final manuscript.

Competing interests. No competing interests are present.

Acknowledgements. This research was supported by the Forecasting Regional Arctic sea ice from a Month to Seasons (FRAMS) project, which is funded by the Marine Environmental Observation, Prediction and Response Network (MEOPAR). This research received additional funding from the Office of Naval Research (ONR-N00014-11-1-0977), the National Science Foundation (NSF-PLR 15-04404), the Canadian Sea Ice and Snow Evolution Network (CanSISE), which is funded by the Natural Science and Engineering and Research Council (NSERC) Climate Change and Atmospheric Research Program. Charles Brunette is grateful for academic and financial support by ArcTrain Canada, McGill University, Québec-Océan, Fonds de recherche du Québec - Nature et technologies and the Norht Slope Borough of Alaska (Eben Hopson Award). We wish to thank Laure Coquart for retrieving and providing the ERA5 data. We thank Rym Msadek and Gunnar Spreen for their input at different stages of the project. Maps were created using the ncpolarm function created by Andrew Roberts (2020), and the function Scatter Plot colored by Kernel Density Estimate by Nils Haëntjens (2020) was also used for creating figures. Arctic dynamic topography/geostrophic currents data were provided by the Centre for Polar Observation and Modelling, University College London.

https://doi.org/10.5194/tc-2021-249
Preprint. Discussion started: 16 August 2021

References

Andersen, S., Tonboe, R., Kaleschke, L., Heygster, G., and Pedersen, L. T.: Intercomparison of passive microwave sea ice concentration retrievals over the high-concentration Arctic sea ice, Journal of Geophysical Research: Oceans, 112, https://doi.org/10.1029/2006JC003543, 2007.

Aporta, C.: Life on the ice: understanding the codes of a changing environment, Polar Record, 38, 341–354, https://doi.org/10.1017/S0032247400018039, 2002.

Armitage, T. W., Bacon, S., Ridout, A. L., Petty, A. A., Wolbach, S., and Tsamados, M.: Arctic Ocean surface geostrophic circulation 2003-2014, The Cryosphere, 11, 1767–1780, https://doi.org/10.5194/tc-11-1767-2017, 2017.

Armitage, T. W., Manucharyan, G. E., Petty, A. A., Kwok, R., and Thompson, A. F.: Enhanced eddy activity in the Beaufort Gyre in response to sea ice loss, Nature communications, 11, 1–8, https://doi.org/10.1038/s41467-020-14449-z, 2020.

Belter, H. J., Krumpen, T., von Albedyll, L., Alekseeva, T. A., Frolov, S. V., Hendricks, S., Herber, A., Polyakov, I., Raphael, I., Ricker, R., et al.: Interannual variability in Transpolar Drift ice thickness and potential impact of Atlantification, The Cryosphere Discussions, pp. 1–24, https://doi.org/10.5194/tc-2020-305, 2020.

Bouchat, A. and Tremblay, B.: Energy dissipation in viscous-plastic sea-ice models, Journal of Geophysical Research: Oceans, 119, 976–994, https://doi.org/10.1002/2013JC009436, 2014.

Brodzik, M. J. and Knowles, K.: EASE-Grid: A versatile set of equal-area projections and grids, Discrete global grids, 2002.

Brunette, C., Tremblay, B., and Newton, R.: Winter Coastal Divergence as a Predictor for the Minimum Sea Ice Extent in the Laptev Sea, Journal of Climate, 32, 1063–1080, https://doi.org/10.1175/JCLI-D-18-0169.1, 2019.

Campbell, G., Pfirman, S., Tremblay, B., Newton, R., Meier, W., and Fowler, C.: Sea Ice tracking utility, digital media, [Available online at http://icemotion.labs.nsidc.org/SITU/], 2020.

Castellani, G., Losch, M., Ungermann, M., and Gerdes, R.: Sea-ice drag as a function of deformation and ice cover: Effects on simulated sea ice and ocean circulation in the Arctic, Ocean Modelling, 128, 48–66, https://doi.org/10.1016/j.ocemod.2018.06.002, 2018.

Cavalieri, D. J., Gloersen, P., and Campbell, W. J.: Determination of sea ice parameters with the Nimbus 7 SMMR, Journal of Geophysical Research: Atmospheres, 89, 5355–5369, https://doi.org/10.1029/JD089iD04p05355, 1984.

Comiso, J. C.: Characteristics of Arctic winter sea ice from satellite multispectral microwave observations, Journal of Geophysical Research: Oceans, 91, 975–994, https://doi.org/10.1029/JC091iC01p00975, 1986.

Copernicus Climate Change Service: ERA5: Fifth generation of ECMWF atmospheric reanalyses of the global climate, 2017.

Darby, D. A.: Arctic perennial ice cover over the last 14 million years, Paleoceanography, 23, https://doi.org/10.1029/2007PA001479, 2008.

Emery, W., Fowler, C., and Maslanik, J.: Satellite Remote Sensing of Ice Motion, in: Oceanographic applications of remote sensing, edited by Ikeda, M. and Dobson, F. W., CRC press, 1995.

Fukumori, I., Wang, O., Fenty, I., Forget, G., Heimbach, P., and Ponte, R. M.: ECCO version 4 release 4, Tech. rep., 2019.

Giles, K. A., Laxon, S. W., Ridout, A. L., Wingham, D. J., and Bacon, S.: Western Arctic Ocean freshwater storage increased by wind-driven spin-up of the Beaufort Gyre, Nature Geoscience, 5, 194–197, https://doi.org/10.1038/NGEO1379, 2012.

Graham, R. M., Cohen, L., Ritzhaupt, N., Segger, B., Graversen, R. G., Rinke, A., Walden, V. P., Granskog, M. A., and Hudson, S. R.: Evaluation of six atmospheric reanalyses over Arctic sea ice from winter to early summer, Journal of Climate, 32, 4121–4143, https://doi.org/10.1175/JCLI-D-18-0643.1, 2019.

Harder, M. and Fischer, H.: Sea ice dynamics in the Weddell Sea simulated with an optimized model, Journal of Geophysical Research: Oceans, 104, 11 151–11 162, https://doi.org/10.1029/1999JC900047, 1999.

Hibler, W.: A dynamic thermodynamic sea ice model, Journal of physical oceanography, 9, 815–846, https://doi.org/10.1175/1520-0485(1979)009<0815:ADTSIM>2.0.CO;2, 1979.

Hongwei, H., Ruibo, L., Peng, L., and Zhijun, L.: Features of sea ice motion observed with ice buoys from the central Arctic Ocean to Fram Strait, Advances in Polar Science, pp. 26–35, https://doi.org/10.13679/j.advps.2019.0020, 2020.

Hwang, B.: Inter-comparison of satellite sea ice motion with drifting buoy data, International Journal of Remote Sensing, 34, 8741–8763, https://doi.org/10.1080/01431161.2013.848309, 2013.

International Arctic Buoy Programme: International Arctic Buoy Programme, digital media, accessed January 2020, [Available online at http://iabp.apl.washington.edu/index.html], 2020.

Inuksuk, A.: On the nature of sea ice around Igloolik, The Canadian Geographer/Le Géographe canadien, 55, 36–41, https://doi.org/10.1111/j.1541-0064.2010.00343.x, 2011.

Kalnay, E., Kanamitsu, M., Kistler, R., Collins, W., Deaven, D., Gandin, L., Iredell, M., and Joseph, D.: The NCEP/NCAR 40-year reanalysis project, Am. Meteorol. Soc, 77, 437–471, https://doi.org/10.1175/1520-0477(1996)077<0437:TNYRP>2.0.CO;2, 1996.

Kimura, N. and Wakatsuchi, M.: Relationship between sea-ice motion and geostrophic wind in the Northern Hemisphere, Geophysical Research Letters, 27, 3735–3738, https://doi.org/10.1029/2000GL011495, 2000.

Krishfield, R. A., Proshutinsky, A., Tateyama, K., Williams, W. J., Carmack, E. C., McLaughlin, F. A., and Timmermans, M.-L.: Deterioration of perennial sea ice in the Beaufort Gyre from 2003 to 2012 and its impact on the oceanic freshwater cycle, Journal of Geophysical Research: Oceans, 119, 1271–1305, https://doi.org/10.1002/2013JC008999, 2014.

Krumpen, T.: AWI ICETrack: Antarctic and Arctic Sea Ice Monitoring and Tracking Tool, Vers. 1.3, 2018.

Krumpen, T., Janout, M., Hodges, K. I., Gerdes, R., Girard-Ardhuin, F., Hölemann, J. A., and Willmes, S.: Variability and trends in Laptev Sea ice outflow between 1992-2011, The Cryosphere, 7, 349–363, https://doi.org/10.5194/tc-7-349-2013, 2013.

Krumpen, T., Gerdes, R., Haas, C., Hendricks, S., Herber, A., Selyuzhenok, V., Smedsrud, L., and Spreen, G.: Recent summer sea ice thickness surveys in Fram Strait and associated ice volume fluxes, The Cryosphere, 10, 523–534, https://doi.org/10.5194/tc-10-523-2016, 2016.

Krupnik, I., Aporta, C., Gearheard, S., Laidler, G. J., and Holm, L. K.: SIKU: knowing our ice, Springer, 2010.

Kwok, R., Schweiger, A., Rothrock, D., Pang, S., and Kottmeier, C.: Sea ice motion from satellite passive microwave imagery assessed with ERS SAR and buoy motions, Journal of Geophysical Research: Oceans, 103, 8191–8214, https://doi.org/10.1029/97JC03334, 1998.

Kwok, R., Spreen, G., and Pang, D.: Arctic sea ice circulation and drift speed: Decadal trends and ocean currents, J. Geophys. Res.: Oceans, 118, 2408–2425, https://doi.org/10.1002/jgrc.20191, 2013.

Lavergne, T., Eastwood, S., Teffah, Z., Schyberg, H., and Breivik, L.-A.: Sea ice motion from low-resolution satellite sensors: An alternative method and its validation in the Arctic, J. Geophys. Res., C10032, https://doi.org/10.1029/2009JC005958, 2013.

Laxon, S. W., Giles, K. A., Ridout, A. L., Wingham, D. J., Willatt, R., Cullen, R., Kwok, R., Schweiger, A., Zhang, J., Haas, C., et al.: CryoSat-2 estimates of Arctic sea ice thickness and volume, Geophysical Research Letters, 40, 732–737, 2013.

Leppäranta, M.: The drift of sea ice, Springer Science & Business Media, 2011.

Lind, S., Ingvaldsen, R. B., and Furevik, T.: Arctic warming hotspot in the northern Barents Sea linked to declining sea-ice import, Nature climate change, 8, 634–639, https://doi.org/10.1038/s41558-018-0205-y, 2018.

https://doi.org/10.5194/tc-2021-249
Preprint. Discussion started: 16 August 2021

Lindsay, R. and Zhang, J.: Assimilation of ice concentration in an ice–ocean model, Journal of Atmospheric and Oceanic Technology, 23, 742–749, https://doi.org/10.1175/JTECH1871.1, 2006.

Lu, P., Li, Z., Cheng, B., and Leppäranta, M.: A parameterization of the ice-ocean drag coefficient, Journal of Geophysical Research: Oceans, 116, https://doi.org/10.1029/2010JC006878, 2011.

Lu, P., Li, Z., and Han, H.: Introduction of parameterized sea ice drag coefficients into ice free-drift modeling, Acta Oceanologica Sinica, 35, 53–59, https://doi.org/10.1007/s13131-016-0796-y, 2016.

Lüpkes, C. and Gryanik, V. M.: A stability-dependent parametrization of transfer coefficients for momentum and heat over polar sea ice to be used in climate models, Journal of Geophysical Research: Atmospheres, 120, 552–581, https://doi.org/10.1002/2014JD022418, 2015.

Maeda, K., Kimura, N., and Yamaguchi, H.: Temporal and spatial change in the relationship between sea-ice motion and wind in the Arctic, Polar Research, 39, 10–33 265, https://doi.org/10.33265/polar.v39.3370, 2020.

Mahoney, A. R., Hutchings, J. K., Eicken, H., and Haas, C.: Changes in the Thickness and Circulation of Multiyear Ice in the Beaufort Gyre Determined From Pseudo-Lagrangian Methods from 2003–2015, Journal of Geophysical Research: Oceans, 124, 5618–5633, https://doi.org/10.1029/2018JC014911, 2019.

McPhee, M. G.: An analysis of pack ice drift in summer, Sea ice processes and models, pp. 62–75, 1980.

McPhee, M. G.: Intensification of geostrophic currents in the Canada Basin, Arctic Ocean, Journal of climate, 26, 3130–3138, https://doi.org/10.1175/JCLI-D-12-00289.1, 2013.

Meier, W., Fetterer, F., Savoie, M., Mallory, S., Duerr, R., and Stroeve, J.: NOAA/NSIDC Climate Data Record of Passive Microwave Sea Ice Concentration, Version 3, digital media, accessed November 2017, doi:10.7265/N59P2ZTG, 2017.

Meier, W. N. and Dai, M.: High-resolution sea-ice motions from AMSR-E imagery, Annals of Glaciology, 44, 352–356, https://doi.org/10.3189/172756406781811286, 2006.

Meneghello, G., Marshall, J., Campin, J.-M., Doddridge, E., and Timmermans, M.-L.: The ice-ocean governor: Ice-ocean stress feedback limits Beaufort Gyre spin-up, Geophysical Research Letters, 45, 11–293, https://doi.org/10.1029/2018GL080171, 2018.

Mercator Ocean: Mercator Ocean GLORYS2V4 Reanalysis, 2017.

Nansen, F.: The Norwegian North polar expedition, 1893-1896: scientific results, vol. 6, Longmans, Green and Company, 1902.

Newton, R., Pfirman, S., Tremblay, B., and DeRepentigny, P.: Increasing transnational sea-ice exchange in a changing Arctic Ocean, Earth's Future, 5, 633–647, https://doi.org/10.1002/2016EF000500, 2017.

Nikolaeva, A. J. and Sesterikov, N. P.: A method of calculation of ice conditions (on the example of the Laptev Sea), vol. 74, Amerind Publishing, 1970.

Nøst, O. A. and Isachsen, P. E.: The large-scale time-mean ocean circulation in the Nordic Seas and Arctic Ocean estimated from simplified dynamics, Journal of Marine Research, 61, 175–210, https://doi.org/10.1357/002224003322005069, 2003.

Olason, E. and Notz, D.: Drivers of variability in A rctic sea-ice drift speed, Journal of Geophysical Research: Oceans, 119, 5755–5775, https://doi.org/10.1002/ 2014JC009897, 2014.

Park, H.-S. and Stewart, A.: An analytical model for wind-driven Arctic summer sea ice drift, The Cryosphere, 10, 227–244, https://doi.org/10.5194/tc-10-227-2016, 2016.

Pfirman, S., Haxby, W., Eicken, H., Jeffries, M., and Bauch, D.: Drifting Arctic sea ice archives changes in ocean surface conditions, Geophysical Research Letters, 31, https://doi.org/10.1029/2004GL020666, 2004.

https://doi.org/10.5194/tc-2021-249
Preprint. Discussion started: 16 August 2021

Polyak, L., Alley, R. B., Andrews, J. T., Brigham-Grette, J., Cronin, T. M., Darby, D. A., Dyke, A. S., Fitzpatrick, J. J., Funder, S., Holland, M., et al.: History of sea ice in the Arctic, Quaternary Science Reviews, 29, 1757–1778, https://doi.org/10.1016/j.quascirev.2010.02.010, 2010.

Proshutinsky, A., Krishfield, R., Toole, J., Timmermans, M.-L., Williams, W., Zimmermann, S., Yamamoto-Kawai, M., Armitage, T., Dukhovskoy, D., Golubeva, E., et al.: Analysis of the Beaufort Gyre freshwater content in 2003–2018, Journal of Geophysical Research: Oceans, 124, 9658–9689, https://doi.org/10.1029/2019JC015281, 2019.

Rabinovich, A. B., Shevchenko, G. V., and Thomson, R. E.: Sea ice and current response to the wind: A vector regressional analysis approach, Journal of atmospheric and oceanic technology, 24, 1086–1101, https://doi.org/10.1175/JTECH2015, 2007.

Rampal, P., Weiss, J., and Marsan, D.: Positive trend in the mean speed and deformation rate of Arctic sea ice, 1979–2007, Journal of Geophysical Research: Oceans, 114, https://doi.org/10.1029/2008JC005066, 2009.

Regan, H., Lique, C., Talandier, C., and Meneghello, G.: Response of Total and Eddy Kinetic Energy to the Recent Spinup of the Beaufort Gyre, Journal of Physical Oceanography, 50, 575–594, https://doi.org/10.1175/JPO-D-19-0234.1, 2020.

Regan, H. C., Lique, C., and Armitage, T. W.: The Beaufort Gyre extent, shape, and location between 2003 and 2014 from satellite observations, Journal of Geophysical Research: Oceans, 124, 844–862, https://doi.org/https://doi.org/10.1029/2018JC014379, 2019.

Rothrock, D., Percival, D., and Wensnahan, M.: The decline in arctic sea-ice thickness: Separating the spatial, annual, and interannual variability in a quarter century of submarine data, Journal of Geophysical Research: Oceans, 113, https://doi.org/10.1029/2007JC004252, 2008.

Schweiger, A., Lindsay, R., Zhang, J., Steele, M., Stern, H., and Kwok, R.: Uncertainty in modeled Arctic sea ice volume, Journal of Geophysical Research: Oceans, 116, https://doi.org/10.1029/2011JC007084, 2011.

Steiner, N.: Introduction of variable drag coefficients into sea-ice models, Annals of Glaciology, 33, 181–186, https://doi.org/10.3189/172756401781818149, 2001.

Sumata, H., Lavergne, T., Girard-Ardhuin, F., Kimura, N., Tschudi, M. A., Kauker, F., Karcher, M., and Gerdes, R.: An intercomparison of Arctic ice drift products to deduce uncertainty estimates, Journal of Geophysical Research: Oceans, 119, 4887–4921, https://doi.org/10.1002/ 2013JC009724, 2014.

Tandon, N. F., Kushner, P. J., Docquier, D., Wettstein, J. J., and Li, C.: Reassessing Sea Ice Drift and Its Relationship to Long-Term Arctic Sea Ice Loss in Coupled Climate Models, Journal of Geophysical Research: Oceans, 123, 4338–4359, https://doi.org/10.1029/2017JC013697, 2018.

Thomas, D.: The quality of sea ice velocity estimates, Journal of Geophysical Research: Oceans, 104, 13 627–13 652, https://doi.org/10.1029/1999JC900086, 1999.

Thorndike, A. and Colony, R.: Sea ice motion in response to geostrophic winds, Journal of Geophysical Research: Oceans, 87, 5845–5852, https://doi.org/10.1029/JC087iC08p05845, 1982.

Togunov, R. R., Klappstein, N. J., Lunn, N. J., Derocher, A. E., and Auger-Méthé, M.: Opportunistic evaluation of modelled sea ice drift using passively drifting telemetry collars in Hudson Bay, Canada, The Cryosphere, 14, 1937–1950, https://doi.org/10.5194/tc-14-1937-2020, 2020.

Tremblay, L., Schmidt, G., Pfirman, S., Newton, R., and DeRepentigny, P.: Is ice-rafted sediment in a North Pole marine record evidence for perennial sea-ice cover?, Phil. Trans. R. Soc. A, 373, 20140168, https://doi.org/10.1098/rsta.2014.0168, 2015.

https://doi.org/10.5194/tc-2021-249
Preprint. Discussion started: 16 August 2021

Tsamados, M., Feltham, D. L., Schroeder, D., Flocco, D., Farrell, S. L., Kurtz, N., Laxon, S. W., and Bacon, S.: Impact of variable atmospheric and oceanic form drag on simulations of Arctic sea ice, Journal of Physical Oceanography, 44, 1329–1353, https://doi.org/10.1175/JPO-D-13-0215.1, 2014.

Tschudi, M., Fowler, C., Maslanik, J., and Stroeve, J.: Tracking the movement and changing surface characteristics of Arctic sea ice, IEEE Journal of selected topics in applied earth observations and remote sensing, 3, 536–540, https://doi.org/10.1109/JSTARS.2010.2048305, 2010.

Tschudi, M., Meier, W. N., Stewart, J. S., Fowler, C., and Maslanik, J.: Polar Pathfinder daily 25 km EASE-grid sea ice motion vectors. Version 4., digital media, accessed January 2020, doi:10.5067/INAWUWO7QH7B, 2019.

Uotila, J.: Observed and modelled sea-ice drift response to wind forcing in the northern Baltic Sea, Tellus A, 53, 112–128, https://doi.org/10.1034/j.1600-0870.2001.01172.x, 2001.

Williams, J., Tremblay, B., Newton, R., and Allard, R.: Dynamic preconditioning of the minimum September sea-ice extent, J. Climate, 29, 5879–5891, https://doi.org/10.1175/JCLI-D-15-0515.1, 2016.

Yu, X., Rinke, A., Dorn, W., Spreen, G., Lüpkes, C., Sumata, H., and Gryanik, V. M.: Evaluation of Arctic sea-ice drift and its dependency on near-surface wind and sea-ice concentration and thickness in the coupled regional climate model HIRHAM-NAOSIM, The Cryosphere Discuss., https://doi.org/10.5194/tc-2019-183, 2020.

Zhang, J. and Rothrock, D.: Modeling global sea ice with a thickness and enthalpy distribution model in generalized curvilinear coordinates, Monthly Weather Review, 131, 845–861, https://doi.org/10.1175/1520-0493(2003)131<0845:MGSIWA>2.0.CO;2, 2003.

https://doi.org/10.5194/tc-2021-249
Preprint. Discussion started: 16 August 2021

The Cryosphere
Discussions
Open Access
EGU

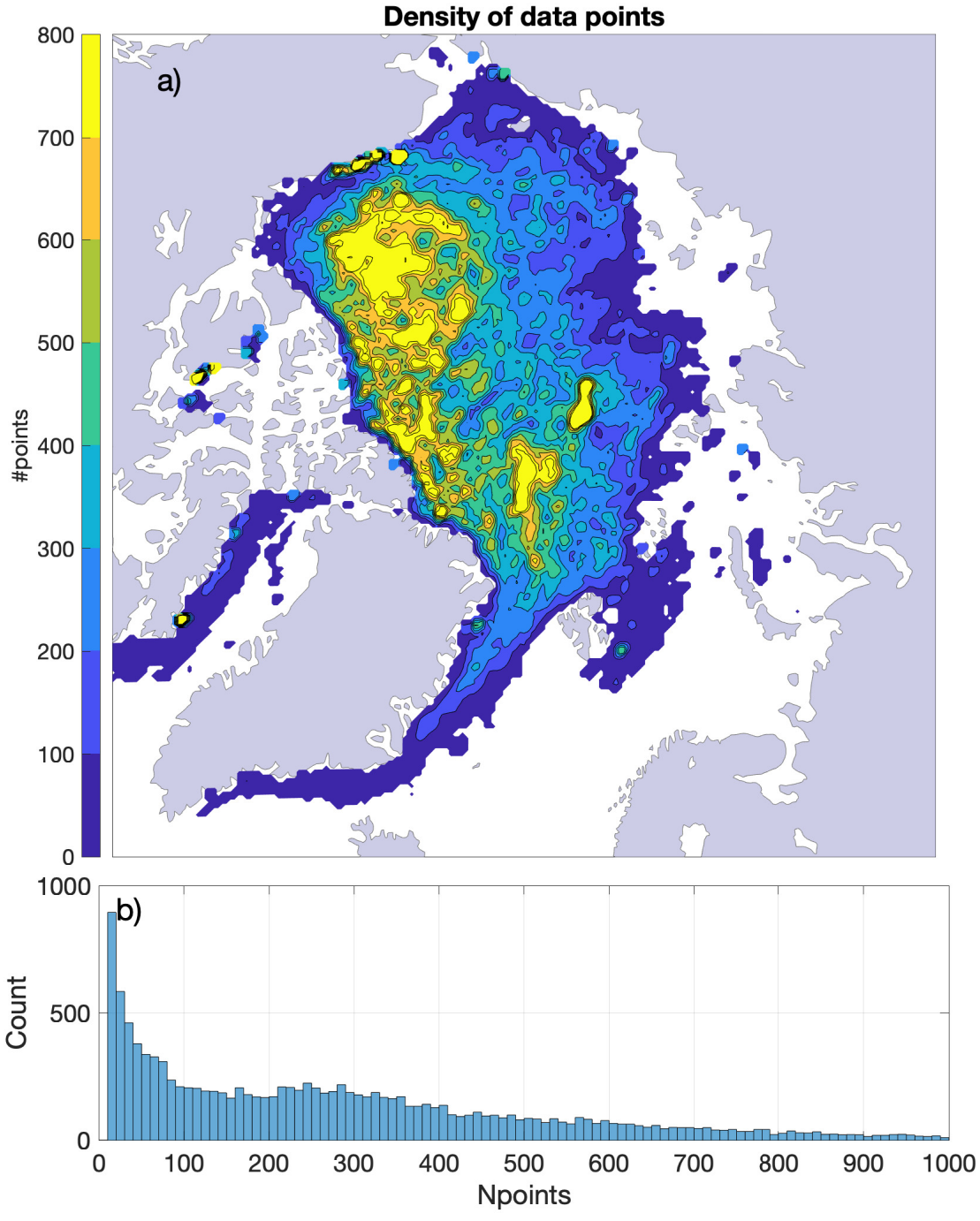

Figure 1. a) Spatial map of the number of data points used for the evaluation of the surface currents $\boldsymbol{U}_w$ at every grid location. b) Distribution of the number of points in grid cells.

https://doi.org/10.5194/tc-2021-249
Preprint. Discussion started: 16 August 2021

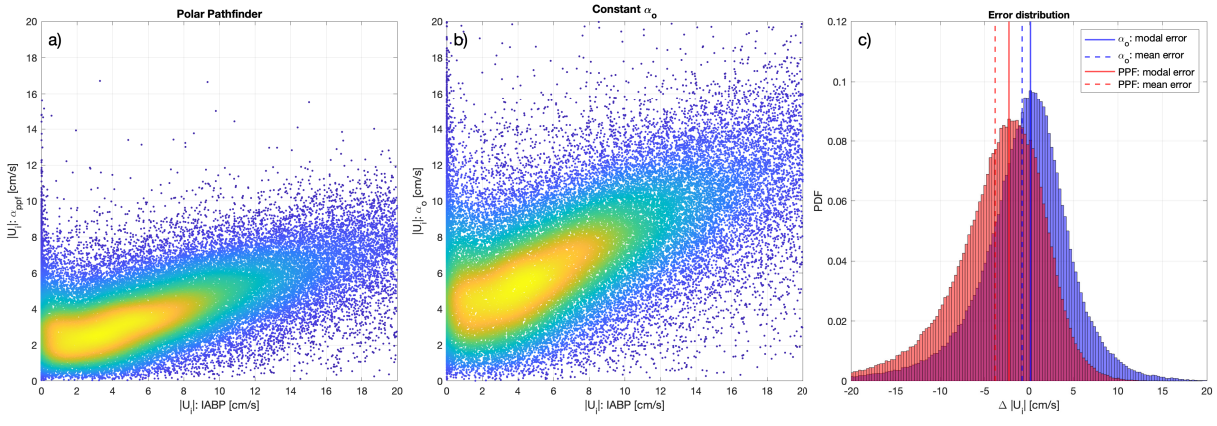

Figure 2. Scatter plot of free drift sea ice speed estimates against buoy ice drift speed for: a) the NSIDC Polar Pathfinder free drift data, and b) for linear free drift with an optimized wind-ice transfer coefficient (no ocean currents). The color scale indicates the density of points on the scatter plot (kernel density estimate). The distribution of the error with respect to the buoy data is shown in c), the solid lines indicate the modal histogram bin; the dashed line indicates the mean error.

https://doi.org/10.5194/tc-2021-249
Preprint. Discussion started: 16 August 2021

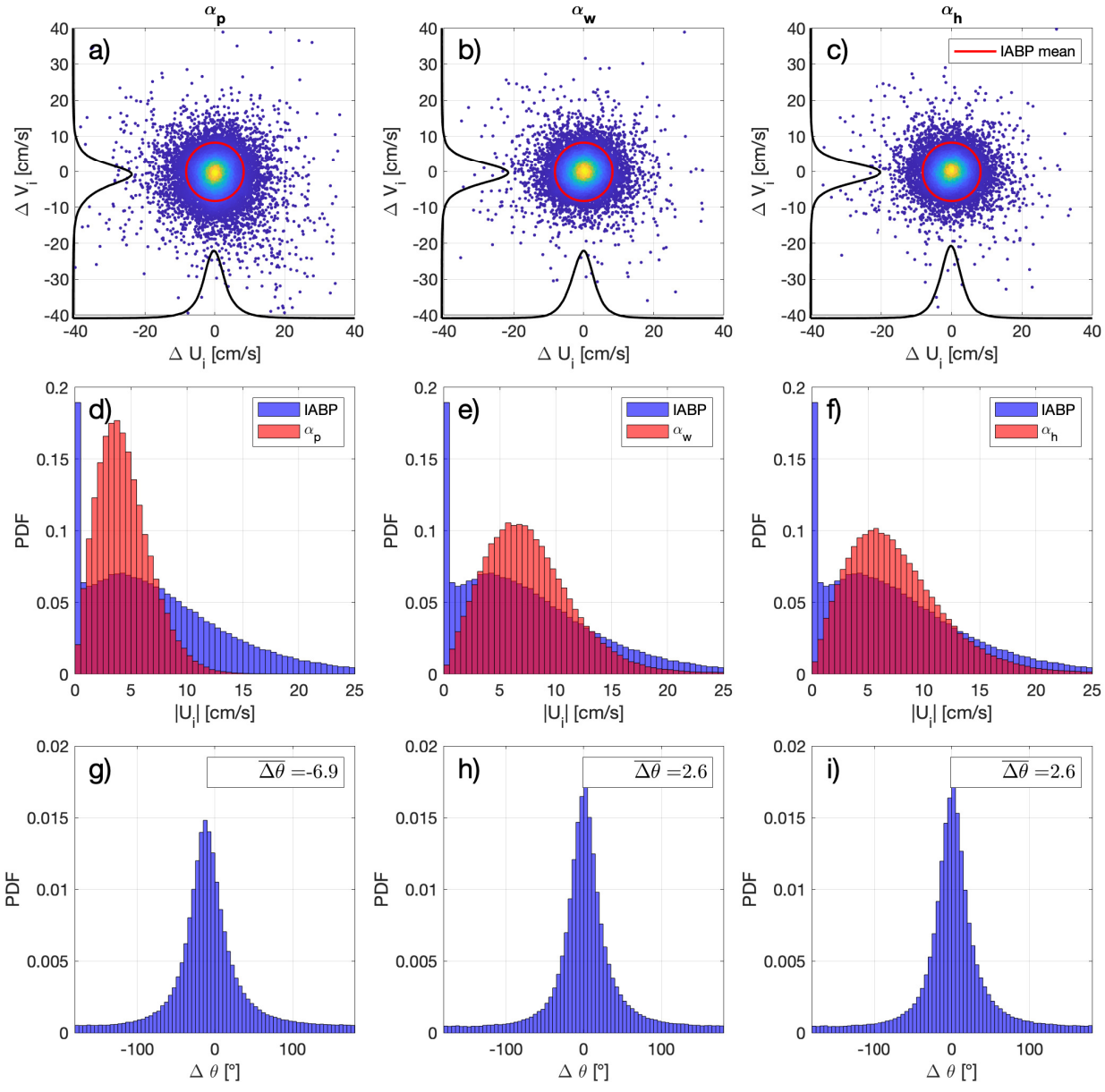

Figure 3. Error metrics for the the α_p Polar Pathfinder (left column), constant α_0 free drift (middle column), and α_h thickness dependent free drift parameterization (right column), taking the IABP buoys as the reference. a),b) and c) show a scatter plot of the error on the u- and v-components of sea ice velocity, where the color scale indicates the density of points, the red circle has a radius equal to the mean buoy drift speed, and the black curves illustrates the distribution of the error in each direction. d), e) and f) show the distribution of the sea ice drift speed for the buoy data (blue) and for each of the free drift parameterization (red). g), h) and i) show the distribution of the drift direction error. All data over the 1979-2019 period is included.

https://doi.org/10.5194/tc-2021-249
Preprint. Discussion started: 16 August 2021

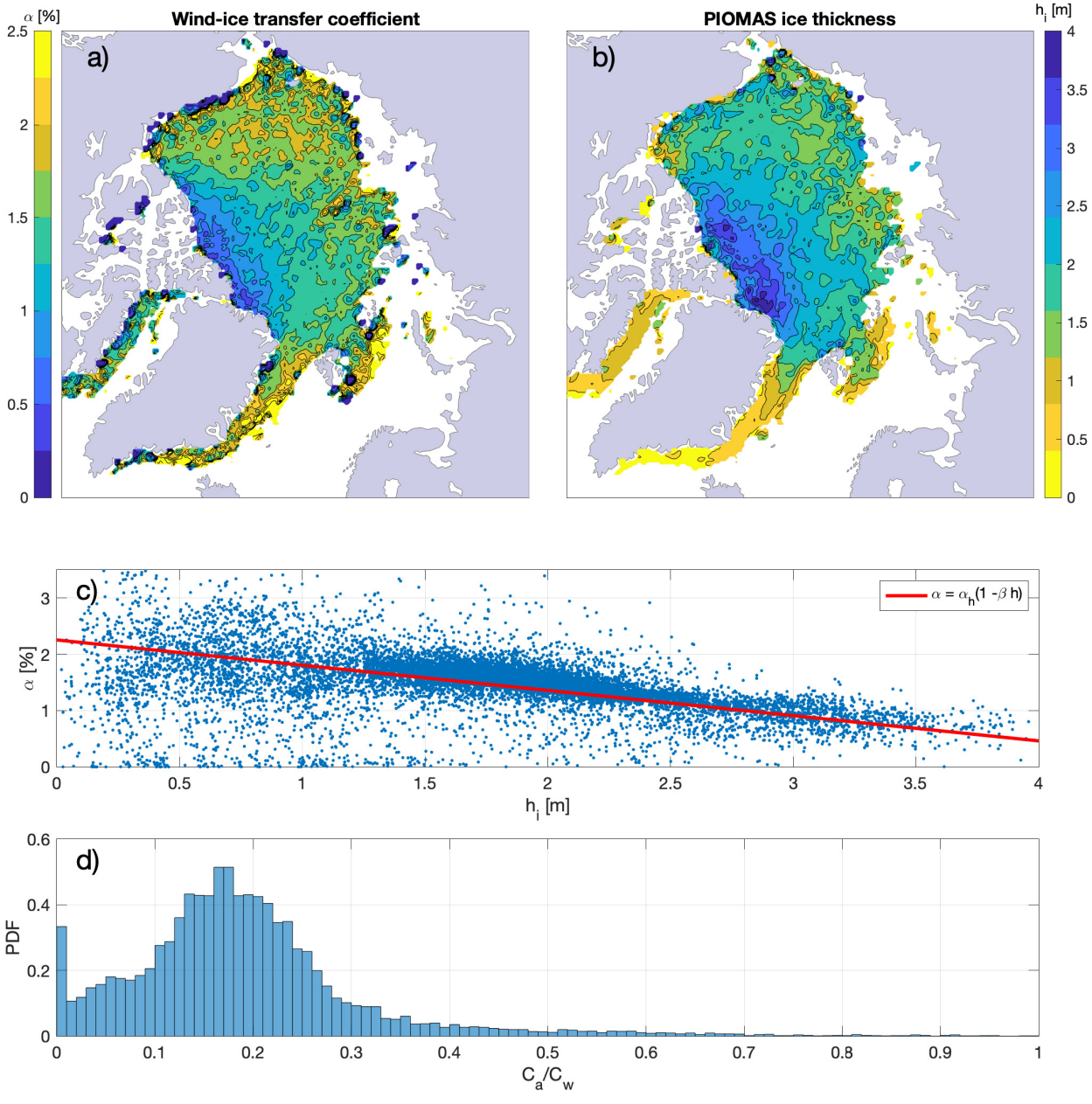

Figure 4. Spatial distribution of: a) wind-ice transfer coefficient calculated as the ratio between the buoy ice velocity and the 10m wind velocity, b) PIOMAS ice thickness (at buoy location). For each grid cell, all data over the 1979-2019 period within a 3x3 search array centered on each grid cell is considered. These fields therefore representing year-round climatological averages. c) scatter plot of the magnitude of the transfer coefficient against ice thickness; the red line indicates the best linear fit. d) distribution of the equivalent ratio of atmospheric to ocean drag coefficients, C_a/C_w.

https://doi.org/10.5194/tc-2021-249
Preprint. Discussion started: 16 August 2021

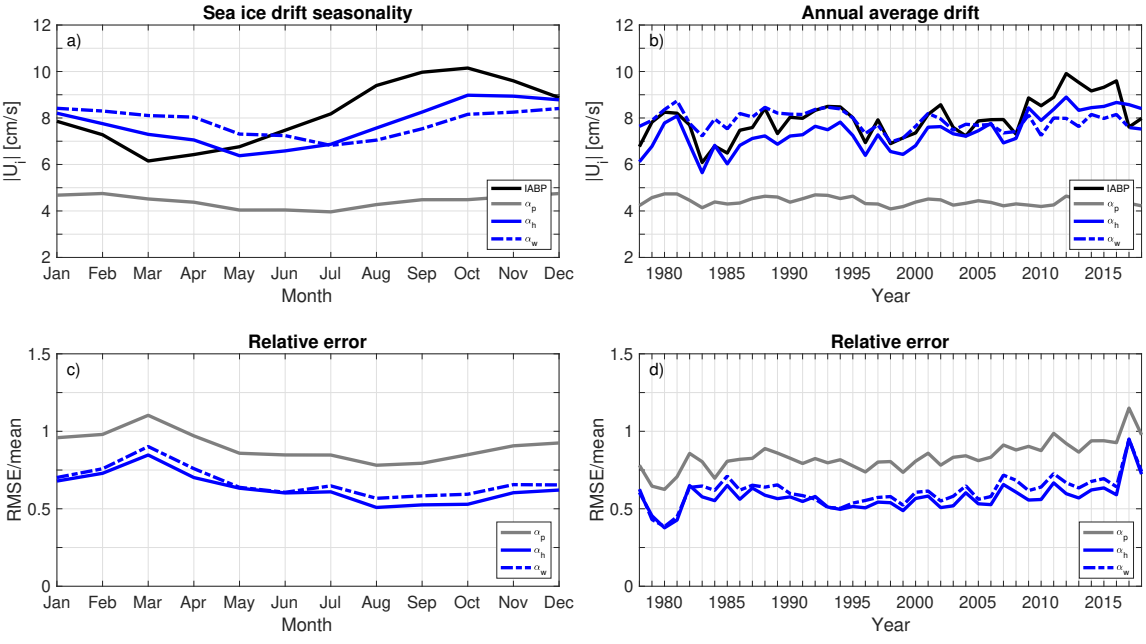

Figure 5. Comparison between the IABP buoy drifts and the Polar Pathfinder free drift component (α_p, grey), free drift including a dependence on sea ice thickness (α_h, blue) and free drift using a constant transfer coefficient (α_w, dashed blue). Free drift estimates are made at all buoy locations. a) Seasonal cycle of monthly sea ice drift speed averaged over the 1979-2019 period, b) Time series of the annual averaged sea ice drift speed, c) seasonal and d) time series of the relative error. The relative error is defined as the root-mean-square error weighted by the mean buoy drift speed.

https://doi.org/10.5194/tc-2021-249
Preprint. Discussion started: 16 August 2021

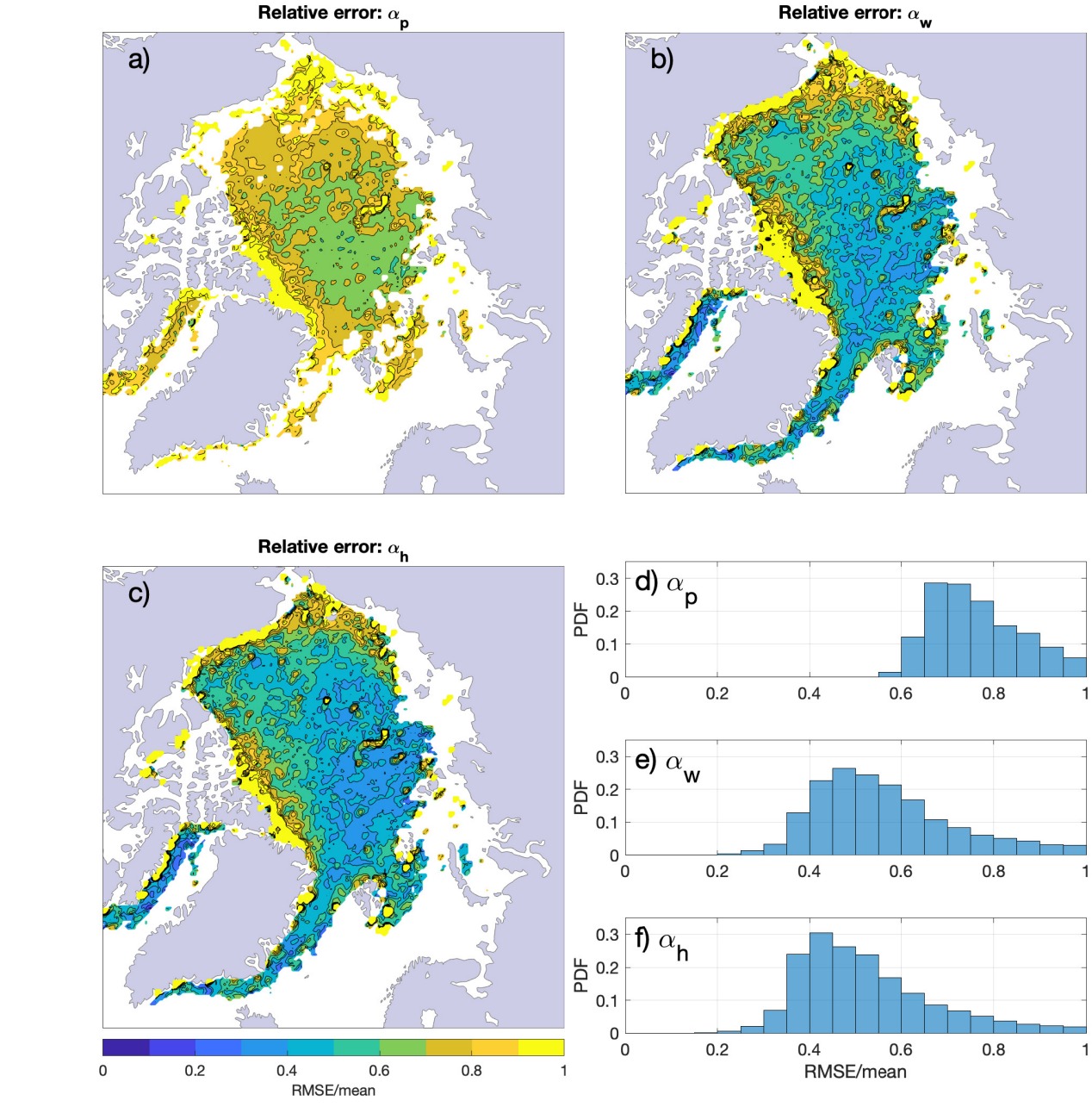

Figure 6. Spatial distribution of the relative error, defined as the root-mean-square error between free drift estimates and the IABP buoy drift, weighted by the mean buoy drift speed, for a) Polar Pathfinder free drift component α_p, b) constant wind-ice transfer coefficient α_w and c) thickness dependent free drift α_h. All data points over the 1979-2019 period are included. The distribution of the relative error for each of the free drift estimates is shown in d-e-f.

https://doi.org/10.5194/tc-2021-249
Preprint. Discussion started: 16 August 2021

The Cryosphere
Discussions
Open Access
EGU

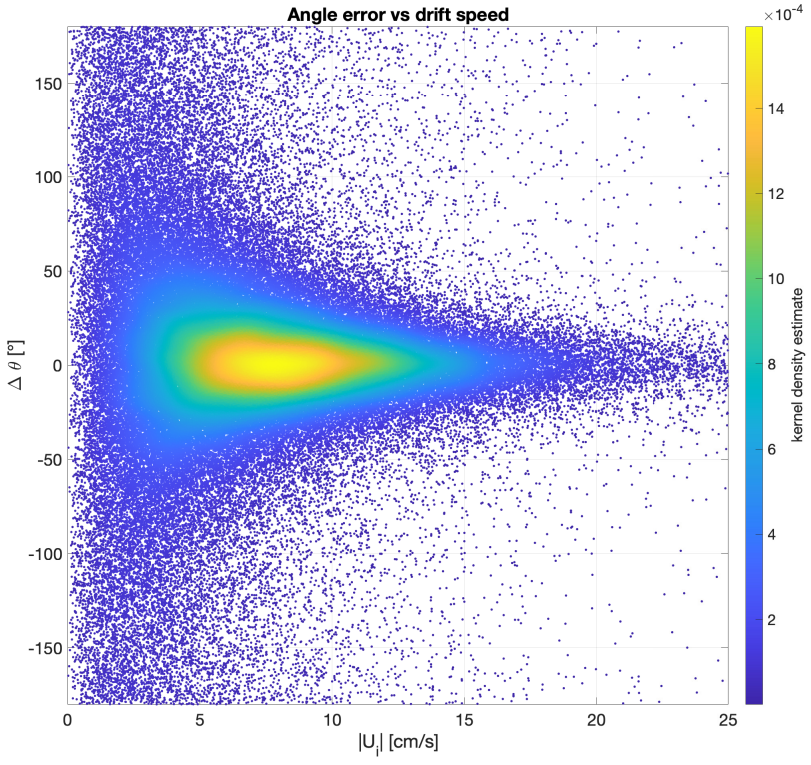

Figure 7. Error on the direction of the drift as a function of the IABP drift speed. The error is taken as the angle between the direction of the free drift estimate (for the thickness-dependent parameterization) and the direction of the buoy drift, for all buoy data available over the 1979-2019 period. The drift angle error takes a value between +180° (free drift is to the left of the buoy drift) and -180° (free drift is to the right of the buoy drift). The color scale represents the kernel density estimate, an indicator of the density of points in the graph.

https://doi.org/10.5194/tc-2021-249
Preprint. Discussion started: 16 August 2021

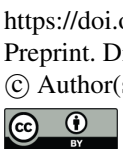

The Cryosphere
Discussions
Open Access
EGU

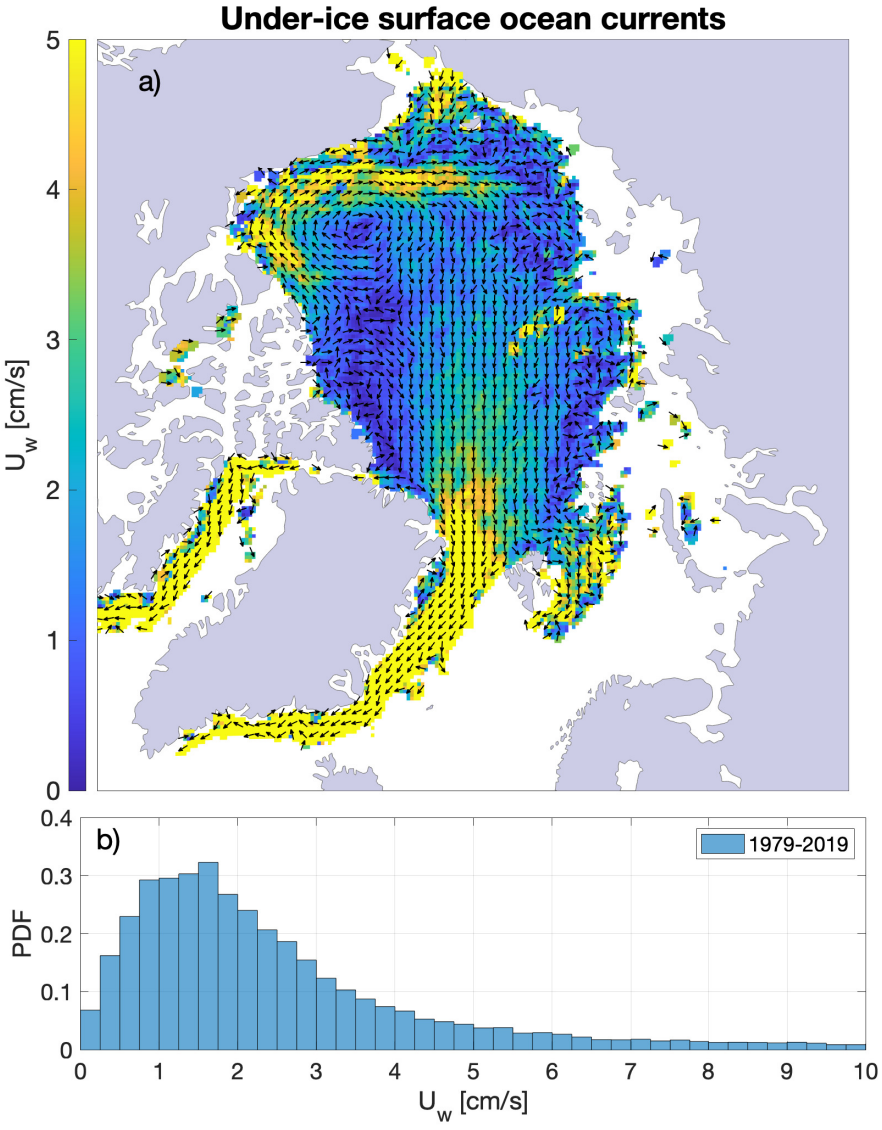

Figure 8. a) Estimates of the oceanic surface currents over the 1979-2019 period; calculated as the ice motion unexplained by the wind, considering the $\alpha(h)$ parameterization for free drift. The distribution of the current speed is presented in b). For any given grid cell, the surface current is taken as the intercept in a best linear fit between the sea ice motion from the IABP buoys and the ERA5 10m winds times the thickness-dependent transfer coefficient.

https://doi.org/10.5194/tc-2021-249
Preprint. Discussion started: 16 August 2021

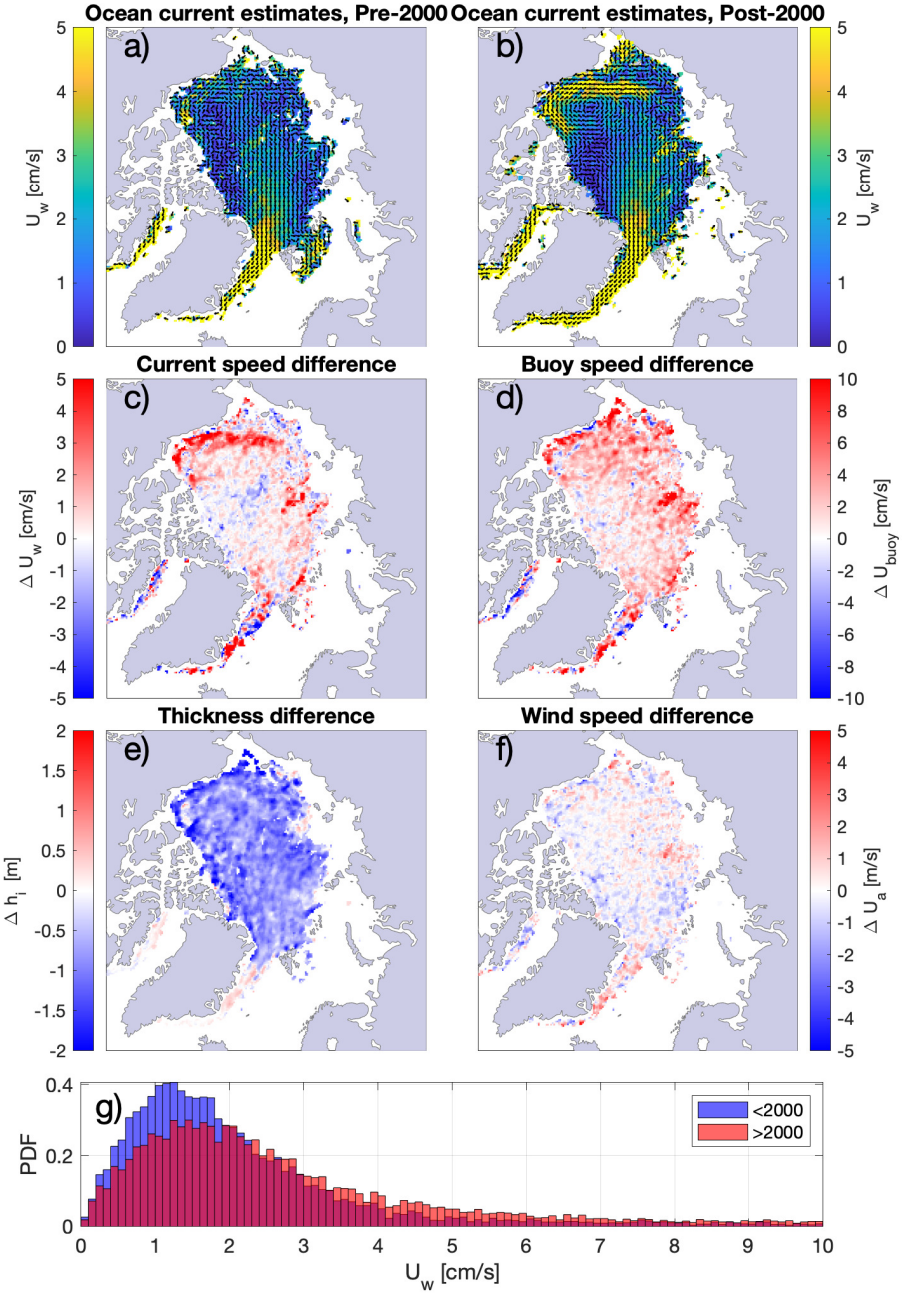

Figure 9. Estimates of the oceanic surface currents for the period covering a) 1979-2000, b) 2001-2019, calculated as in Figure 8. Maps of the difference between the pre-2000 and post-2000 periods are presented for the following fields: c) surface oceanic currents speed, d) buoy-derived ice drift speed, e) ice thickness from PIOMAS, and f) 10m wind speed from ERA5. The distribution of current speed for the pre- and post-2000 periods is presented in g).

https://doi.org/10.5194/tc-2021-249
Preprint. Discussion started: 16 August 2021

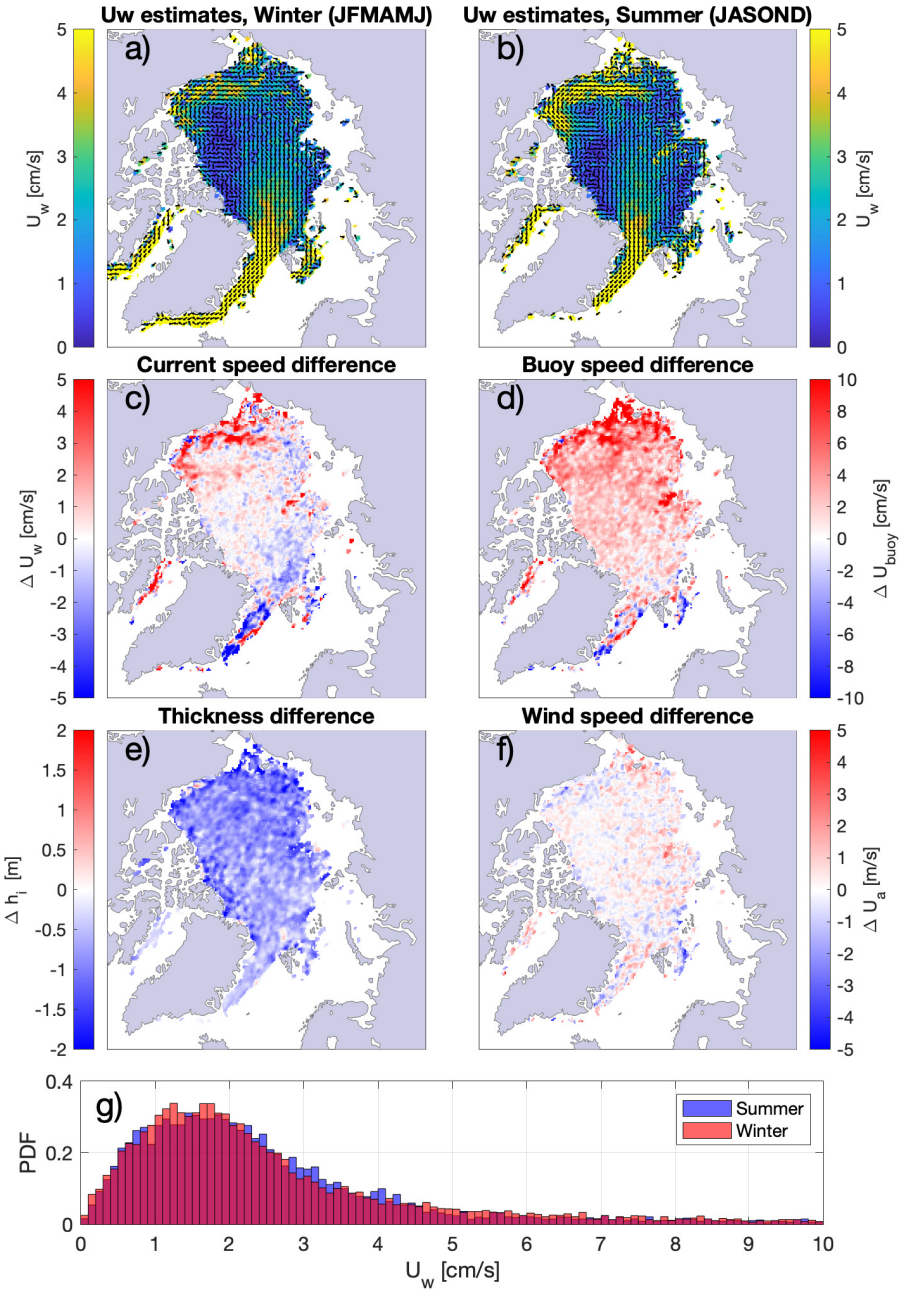

Figure 10. Estimates of the oceanic surface currents for a) the summer season (JASOND) b) the winter season (JFMAMJ). Maps of the difference between the summer and winter are presented for the following fields: c) surface oceanic currents speed, d) buoy-derived ice drift speed, e) ice thickness from PIOMAS, and f) 10m wind speed from ERA5. The distribution of current speed for the summer/winter seasons is presented in g).

https://doi.org/10.5194/tc-2021-249
Preprint. Discussion started: 16 August 2021

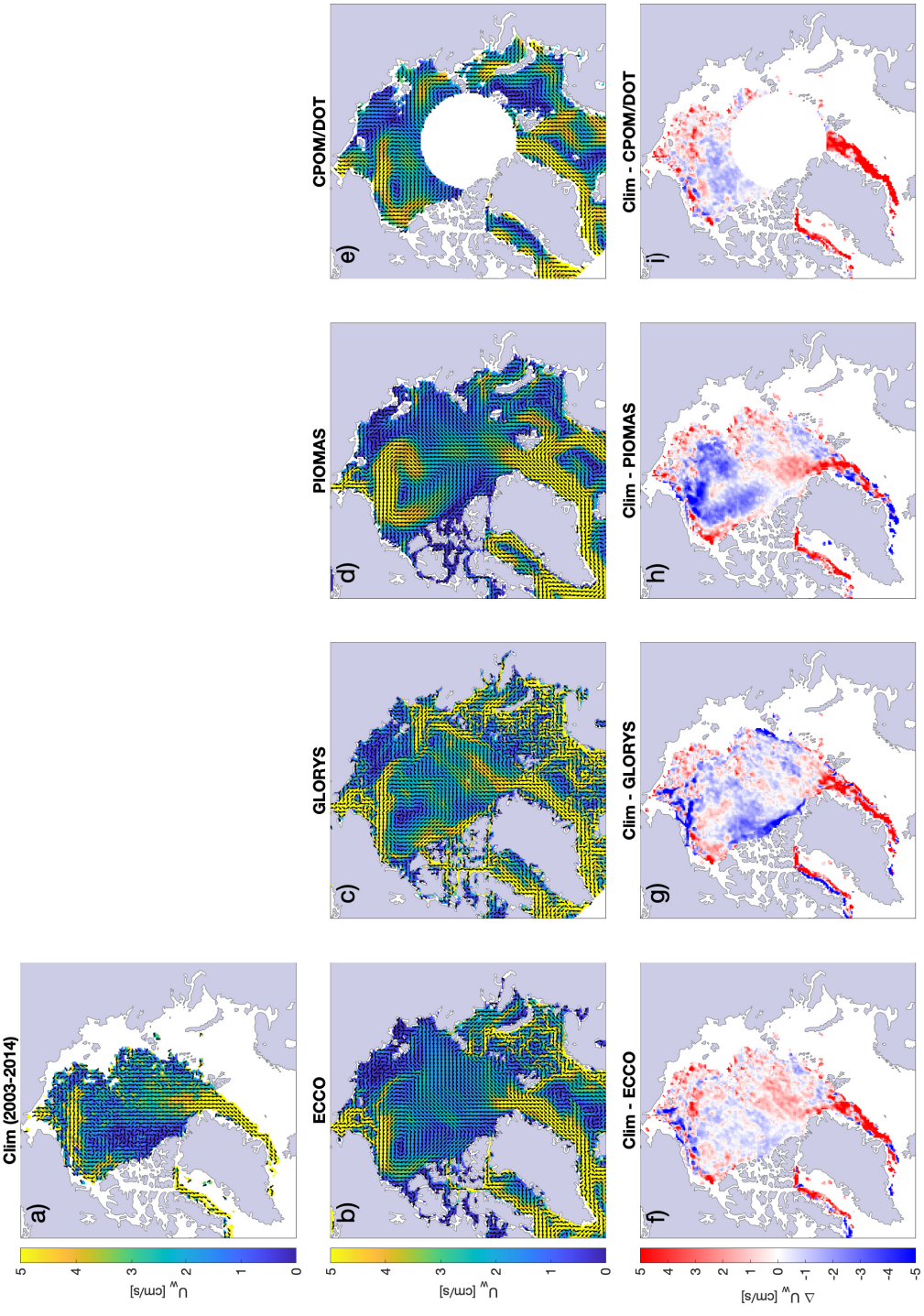

Figure 11. 2003-2014 climatology of the ocean currents from: a) residual from total buoy ice motion, b) ECCO, at a depth of 5 m c) GLORYS, at a depth of 5 m d) PIOMAS, at a depth of 7.5 m and e) geostrophic ocean currents from the dynamic ocean topography. f) through i) shows the difference in velocity between the ocean currents in a) and each of the four other ocean velocity product.